Density functional theory study of the α-γ phase transition in cerium: Role of electron correlation and f-orbital localization

Marco Casadei,[1,2] Xinguo Ren,[1,3] Patrick Rinke,[1,4] Angel Rubio,[1,5,6] and Matthias Scheffler[1]

[1]*Fritz-Haber-Institut der Max-Planck-Gesellschaft, Faradayweg 4-6, D-14195 Berlin, Germany*

[2]*Institute of Condensed Matter and Nanosciences, Université catholique de Louvain, 1348 Louvain-la-neuve, Belgium*

[3]*Key Laboratory of Quantum Information, University of Science and Technology of China, Hefei, Anhui 230026, China*

[4]*COMP/Department of Applied Physics, Aalto University, P.O. Box 11100, Aalto FI-00076, Finland*

[5]*Max Planck Institute for the Structure and Dynamics of Matter, Luruper Chaussee 149, 22761 Hamburg, Germany*

[6]*Center for Free-Electron Laser Science & Department of Physics, University of Hamburg, Luruper Chaussee 149, 22761 Hamburg, Germany*

(Received 22 July 2015; revised manuscript received 5 February 2016; published 29 February 2016)

The long standing problem of the α-γ phase transition in cerium metal is approached by treating all electrons at the same quantum mechanical level, using both hybrid functionals (PBE0 and HSE06) and exact exchange plus correlation in the random-phase approximation (EX+cRPA). The exact-exchange contribution in PBE0 and HSE06 is crucial to produce two distinct solutions that can be associated with the α and γ phases. An analysis of the band structure and the electron density reveals a localization and delocalization behavior of the f electrons in the γ and α phases, respectively. However, a quantitative agreement with the extrapolated phase diagram to zero temperature is achieved only with EX+cRPA, based on the hybrid functional starting point. We predict that a pressure induced phase transition should exist at or close to $T = 0$ K. By adding entropic contributions we determine the pressure-temperature phase diagram, which is in reasonable agreement with experiment.

DOI: 10.1103/PhysRevB.93.075153

I. INTRODUCTION

The first-principles description of f-electron systems, i.e., the rare-earth and actinide materials, is currently regarded as one of the great challenges in condensed matter physics. One prominent example is the description of the volume collapse exhibited by some rare-earth metals [1], where density functional theory (DFT) within its local/semilocal functionals (LDA/GGA) only partially captures the associated phase transitions [2–5].

The isostructural α-γ phase transition in cerium [6] is the most studied case both experimentally and theoretically. Calculations based on density functional theory have so far been unable to produce a double minimum in the total energy versus volume curve, which would be a direct indication of the phase transition, within a single theoretical framework. In recent work [7], we showed that hybrid density functionals [8–10], which incorporate a fraction of exact exchange, yield a double minimum within a single theoretical and computational framework. Agreement with extrapolated experimental results at zero temperature is reached by treating exchange exactly and correlation at the level of the random-phase approximation (denoted as EX+cRPA in this work) [11–14]. Hybrid functionals combined with quantum many-body perturbation techniques appear to be a promising approach for the description of the α-γ transition. In our previous work [7], we obtained two distinctly different solutions, whose structural, electronic, and magnetic properties are consistent with experimental results for the α and γ phases, respectively. Our results not only constituted an investigation of the phase change without adjustable parameters but also provided insight into the nature of the phase transition.

In this work we will further analyze the driving mechanism behind the phase transition, which is to be understood in terms of a *localization/delocalization* competition of the f electrons. By including entropic effects, we will then report a finite temperature phase diagram. The paper is organized as follows: In Sec. II we briefly discuss the motivation behind this work. In Sec. III we provide a detailed review of previous experimental and theoretical work, highlighting the open questions to be addressed in this work. In Sec. IV, the computational approaches used in this work, as well as the implementation details, will be discussed. The results at $T = 0$ K are then presented in Sec. V, first for the bulk α and γ phases and then for finite Ce clusters. Finally in Sec. VI, we present the finite temperature phase diagram for the α-γ phase transition.

II. THE MOTT VERSUS KONDO DEBATE

Cerium undergoes an isostructural (fcc) α-γ phase transition (see Fig. 1), which is accompanied by a volume collapse of 15% at room temperature and ambient pressure [6,15]. In addition to the volume collapse, the phase transition exhibits a change in magnetic properties, from localized magnetic moments, γ phase, to Pauli paramagnetism, α phase, as will be discussed in Sec. III A. While there is no doubt that the f electrons are pivotal for the peculiar behavior of Ce, there is still no consensus on exactly how the f electrons affect the phase transition, despite numerous theoretical and experimental studies.

Initially, a simple *localization-delocalization* scenario was frequently invoked to explain the α-γ phase transition. In γ-cerium (smaller volume) the $4f$ electron resides close to the nucleus. It is unpaired and therefore gives rise to localized magnetic moments. Conversely, in the α phase (larger volume) the f electrons are delocalized and more bandlike and exhibit a typical Pauli paramagnetic behavior. This picture has been supported over the years by many experimental and theoretical studies that have addressed the origin of the transition.

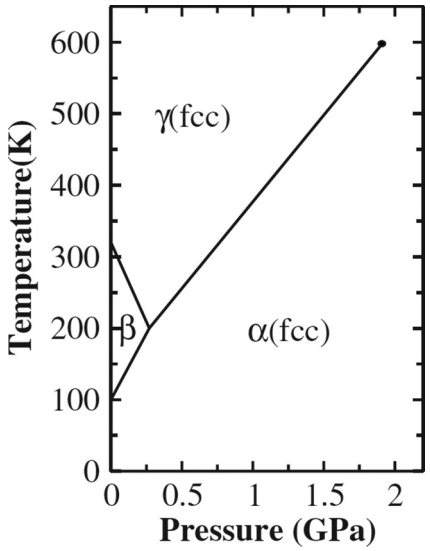

FIG. 1. Experimental phase diagram [6,24] of cerium around the α-γ phase transition. The crystal structure of the α and γ phases is fcc, while the β phase has a double hexagonal closed packed (dhcp) structure.

Nowadays, most studies are based on one of the two prevalent pictures for the driving mechanism of the transition (Sec. III B): the Mott transition [16,17] and the Kondo volume collapse (KVC) [18,19]. The Mott picture involves only the f electrons. It assumes that the competition between the intersite f-f hybridization and the on-site f-f Coulomb interaction is the driving force for the α-γ transition, with f electrons localized in one phase (γ phase) and delocalized in the other (α phase). The spd electrons are only spectators. In the KVC picture, the f electrons are assumed to be localized in both phases. In the KVC model, the f electrons hybridize with the spd electrons, but hopping of f electrons between neighboring sites is not permitted. The change in the screening of the localized moments by the conduction spd electrons induced by the change in volume then triggers the transition.

However, these two scenarios are not as different as people originally thought. Advancement in dynamical mean-field theory (DMFT) [20] revealed that the Hubbard model behind the Mott picture, and the (periodic) Anderson impurity model behind the KVC picture, produce rather similar spectral functions, charge compressibilities, and local magnetic moments across the phase transition [21,22]. This suggests that the two pictures are not completely incompatible, but each model might only capture part of the underlying physics. In fact, Amadon *et al.* [23] recently pointed out that both the intersite f-f hybridization and the f-spd hybridization are important and have to be considered to understand the peculiar properties of Ce.

Models are important in science, as they can aid the interpretation of scientific results and suggest physical processes to be included in our theories. However, they only include a selected set of degrees of freedom, build in the desired physics by hand, and need to be parametrized, which often makes them not material specific. To have an unbiased description of complex phenomena such as the α-γ phase transition, it is desirable to start from *first principles* and treat all electronic degrees of freedom on the same quantum mechanical level. One would expect that the right physics emerges naturally from such first-principles calculations, provided that the underlying approximations for the treatment of exchange and correlation are accurate enough.

In this work we perform density functional calculations with advanced exchange-correlation functional approximations, and provide a *density-based* description of the transition. We thus observe the localization/delocalization process as an outcome of the calculations and do not require it as an input. Our approach cannot capture dynamical processes such as Kondo physics. Therefore it inherently suggests the Mott scenario as the most plausible at zero temperature, but does not rule out the contribution of Kondo physics at higher temperatures. We also suggest that the phase transition is linked to a symmetry breaking, which would manifest itself in a change of the charge density distribution rather than the spin alignment (see Sec. V A).

III. PREVIOUS STUDIES

A. Experimental findings

The α-γ phase transition is accompanied by a change in the magnetic properties of the cerium metal. The magnetic susceptibility of α-Ce as a function of temperature and pressure has been measured by several groups [25–27]. All studies agreed that the α phase is essentially a Pauli paramagnet (i.e., the susceptibility of the material is weak and reflects that of conduction band electrons). However, the value of the susceptibility is 4.5 times higher than the expected Pauli susceptibility. The γ phase of cerium is also a paramagnet. But the magnetic susceptibility obeys the Curie-Weiss law [28–30], indicating the presence of localized magnetic moments.

In 2005 a study from Murani *et al.* [31] argued that the magnetic form factor measured in neutron scattering would correspond to a Ce^{3+} electronic configuration in both phases, suggesting no f-electron delocalization in α-Ce. In the localization/delocalization picture the discrepancy from the ideal Pauli paramagnetism in the α phase could be attributed to a Stoner exchange enhancement [32] arising from an incomplete delocalization of the $4f$ states and a persistence of localized magnetic moments. While there is a reasonable agreement on the observed magnetic properties of cerium, the debate on the existence of an experimental proof for the localization-delocalization process is still ongoing and a consensus has not been reached.

Initially, the question was raised whether the delocalization of the f electrons across the transition would be linked to a promotion of the electrons to the conduction band. However, a first estimation of the number of $4f$ electrons in the α and γ phases, provided by Gustafson *et al.* [33] by means of positron annihilation, showed no change in the number of f electrons going from one phase to the other. The results were then partially confirmed by Compton scattering and neutron scattering measurements [34,35], which estimated $\langle n_f \rangle \simeq 1$ for γ-Ce and $\langle n_f \rangle \simeq 0.8$ for α-Ce.

Subsequently, in 2001, Van der Eb *et al.* [36] provided evidence that the conducting properties of the material would change across the transition even if the number of f electrons

remains constant. The authors studied the optical properties of cerium using ellipsometry and grazing incidence reflectometry. They observed significant changes in the optical conductivity, the dynamical scattering rate, and the carrier effective mass between α- and γ-cerium. In γ-Ce the charge carriers showed a large scattering rate in the far infrared and a carrier mass characteristic of $5d$ band electrons. In α-Ce, a Fermi-liquid frequency-dependent scattering rate was obtained, with an effective mass of the carriers about twenty times that of an electron: three times larger than that in the γ phase. This suggested that the f electrons would remain localized in the α phase, but contribute to the electron conduction via hybridization with the $6s$ and $5d$ electrons.

Numerous other experimental studies have been carried out including photoelectron spectroscopy [37–43], x-ray absorption [44], x-ray photoemission spectroscopy [45–47], and inverse photoelectron spectroscopy [41,47,48]. Electron spectroscopies are highly surface sensitive and this further complicates the understanding of the bulk properties of cerium, where the surface is believed to be of γ nature even in the α phase [42]. Nowadays the results obtained in 1991 by Weschke *et al.* [39] are generally taken as the photoemission spectroscopy reference for cerium. Two main peaks for the f states are found, one around 2 eV below the Fermi level, which is associated with localized electrons, and one at the Fermi level, which is considered originating from delocalized states.

Only a few inverse photoemission spectroscopy (IPES) studies are available for cerium. Results were acquired by Wuilloud *et al.* [47] from a sample of polycrystalline cerium undergoing a temperature driven α-γ phase transition, and by Grioni *et al.* [48], who performed resonant inverse photoemission spectroscopy (RIPES) on thin films. These results revealed a significant difference between the spectra of the α and γ phases near the Fermi level. There are two peaks in the spectra; one is located at the Fermi level, the other one at 4 eV above the Fermi level. These are present in both phases, but the peak at the Fermi level is more pronounced than observed in standard photoemission spectroscopy. Combining the PES and IPES, one obtains the entire energy spectrum of Ce that exhibits the renowned three-peak structure (with peaks at -2 eV, 0 eV, and 4 eV with respect to the Fermi level).

In 2004 Dallera *et al.* [49] and Rueff *et al.* [50] performed bulk-sensitive x-ray absorption (XAS), resonant x-ray emission (RXES), and resonant inelastic x-ray scattering (RIXS) measurements, confirming the presence of the three-peak structure in the spectra. As already observed in IPES, the ratio between the intensity of the peak at 4 eV and the one at the Fermi level exhibit a pronounced drop across the α-γ transition.

Summarizing, there is no conclusive experimental answer regarding the driving mechanism of the volume collapse. Also for the widely discussed localization/delocalization process a true proof has not yet emerged. Even the importance of the f electrons in the α-γ phase transition has been questioned [42].

The role of entropy in the transition was pointed out by some authors [18,51]. Based on experimental data, Amadon *et al.* gave an estimation of the change in Gibbs free energy considering the internal energy (ΔE), as well as entropic ($T\Delta S$) and volume ($p\Delta V$) contributions.

The authors concluded that entropic effects dominate at room temperature, and a study of only the internal energy of the system would not be sufficient for understanding the driving mechanism of the transition. Similar conclusions were reached later by Decremps *et al.* [52].

The entropic change across the transition includes two different contributions, which arise from both lattice vibration and electronic degrees of freedom. The phonon contribution in the α and γ phases was estimated in several studies. In 2004, high-pressure x-ray and neutron diffraction measurements on polycrystalline cerium by Jeong *et al.* [53] suggested a vibrational entropy contribution $\Delta S_{\mathrm{vib}}^{\gamma\text{-}\alpha} \approx 0.75 k_{\mathrm{B}}$ at room temperature, which would account for half of the total entropy change across the transition. The value agreed with earlier estimations of $\Delta S_{\mathrm{vib}}^{\gamma\text{-}\alpha}$ [6] but was in contradiction with the inelastic neutron scattering results of Manley *et al.* on a $Ce_{0.9}Th_{0.1}$ alloy [54], where the change in vibrational entropy was concluded to be negligible. Further analysis was provided by ultrasonic investigations [55,56], where the vibrational contribution to the total entropy change was estimated to be on the order of 15%. A combined high-pressure and high-temperature x-ray diffraction study [15] suggested $\Delta S_{\mathrm{vib}}^{\gamma\text{-}\alpha}/\Delta S_{\mathrm{tot}}^{\gamma\text{-}\alpha} \approx 50\%$. Both values refer to room temperature. In 2011, Krisch *et al.* [57] provided results based on inelastic x-ray scattering. The lattice contribution to the phase transition entropy was found to be around $0.33 k_{\mathrm{B}}$. Using the Clausius-Clapeyron relation $dP/dT = \Delta S_{\mathrm{tot}}^{\gamma\text{-}\alpha}/\Delta V^{\gamma\text{-}\alpha}$, this translates into $\approx$50% of entropic contribution as in previous works. Despite this uncertainty, one thing is clear: Phononic degrees of freedom account for only half of the entropy change at most; the other half has to be of electronic nature.

Also other aspects of the phase transition have been raised. For example, in 2008 and 2011 two studies from Lipp *et al.* [15] and Decremps *et al.* [52] tested the isomorphism of the α and γ phases with respect to the fcc crystal structure. The authors analyzed the volume collapse using high precision x-ray diffraction techniques and excluded a change from the fcc to distorted-fcc structure, which is observed in other lanthanides [58,59]. They performed measurements from room temperature up to 600–800 K, and confirmed the presence of a solid-solid critical point at $T_c \simeq 460$ K and $p_c \simeq 1.5$ GPa.

Motivated by previous theoretical works [60–62] that propose a change in symmetry between the α and γ phases due to an alignment of the charge density along preferred directions, in 2010 Tsvyashchenko *et al.* [63] measured the electric field gradient (EFG) of ^{111}Cd probe nuclei in solid Ce using time-differential perturbed angular correlation spectroscopy. The authors found that the value of the EFG in the α phase is four times larger than in the γ phase. Therefore, the results were interpreted as evidence for quadrupolar electronic charge-density ordering in the α phase and symmetry lowering in the γ-α transition. In this case the nuclei would remain in a face-centered cubic structure in both phases, but the symmetry of the electron density in the α phase would be lower than the symmetry of the fcc crystal.

B. Theoretical models

Two models have been supported as the driving mechanism for the α-γ phase transition (see Sec. II): a Mott transition for the f electrons [16,17] and the Kondo volume collapse

model [18,19]. Johansson [17] has criticized the Kondo volume collapse model based on the slope of the transition line in the P-T phase diagram, which bends upward in contrast to the linearity that has been observed experimentally [6]. A linear behavior is obtained in the framework of the Mott transition. The Mott picture, on the other hand, suffers from inconsistent energy scales [16].

The Kondo scenario is supported by several spectroscopic experimental results [41,47,64,65], but it is challenged by some other photoemission studies [40,66,67]. Probing heavy-fermion compounds containing cerium, which are believed to approximate cerium metal reasonably well and for which the different phases can be explored in wider temperature ranges, Joyce *et al.* [40] in 1992 performed measurements on the localized phase at lower temperatures than the ones available for γ-Ce and observed that the spectral weight of the feature near E_{F}, the *Kondo resonance*, does not scale with T_{K} as expected. However, the conclusions from the authors were criticized by Patthey *et al.* [68] in 1993, who suggested agreement of the same data with the Kondo volume collapse. In 1998 a study by Wesche *et al.* [42] further complicated the situation, showing that, at low temperatures, the photoemission spectra of Ce, characterized by the peak at the Fermi energy, is very similar to that of lanthanum, that has no $4f$ electrons.

Despite the numerous studies that seem to support one or the other model, it appears that a consensus on the nature of the phase transition has not yet been reached. Lipp *et al.* [15] and subsequently Johansson *et al.* [69] were able to reproduce the same P-T phase diagram and the same temperature dependence of the bulk modulus as derived from x-ray diffraction for both the Kondo volume collapse and the Mott transition model.

The Mott transition and Kondo volume collapse have always been considered mutually exclusive, but over the last ten years the view seems to change. For instance, numerical results from dynamical mean-field theory (DMFT) revealed strong analogies between the Hubbard and the periodic Anderson model [21], which are the bases of the two theories, respectively. In 2010, Streltsov *et al.* [70] remarked on the importance of the inclusion of intersite f-f Hubbard-like hybridization in the Anderson impurity calculations for cerium. They argued that for cerium metal the f-f hybridization is comparable to the hybridization between $4f$ and conduction band electrons. They therefore remarked that the best way of approaching cerium would be through the more general Hamiltonian combining both the Hubbard and the periodic Anderson models.

Based on the observation that electron interactions of quadrupolar origin drive symmetry lowering phase transitions in many lanthanide and actinide compounds [71], and following an idea of Eliasbergh and Capellmann [72], Nikolaev and Michel proposed a new driving mechanism for the α-γ phase transition [60–62]. Eliasbergh and Capellmann initially pointed out that a first order phase transition implies a symmetry change according to Landau's theory. This would be related to a not yet observed change in lattice structure from fcc to distorted fcc between the two phases of cerium. However, x-ray diffraction measurements did not provide evidence for such a symmetry breaking, and, in 2008, this hypothesis was excluded by Lipp *et al.* [15]. Nikolaev and Michel then suggested that the phase transition could be accompanied by a special symmetry change from the $Fm\bar{3}m$ to the $Pa\bar{3}$ space group. Usually, a change in the crystal symmetry is due to lattice distortions. According to the authors, however, in the α-γ transition the atomic centers of mass remain in the fcc structure sites for both phases, but the symmetry of the electron density changes across the transition. This means that in one phase the electron density corresponding to the valence orbitals aligns along preferred directions. γ-Ce is the disordered phase, while α-Ce represents the ordered phase. Here, the orientational order is of a quadrupolar nature.

This mechanism would predict a linear increase of the transition temperature with pressure, fixing for instance one of the failures of the Kondo volume collapse model. However, while presenting an attractive alternative to the Mott and Kondo models, Nikolaev and Michel estimated that the symmetry change alone corresponds to a transition energy about two orders of magnitude smaller than the observed one [61]. They therefore refined the theory, adding an on-site Hubbard-like repulsion term for the f electrons and hybridization between f and conduction states in the spirit of the Anderson impurity Hamiltonian [62]. They suggested that the change in symmetry could be the driving force of a further energetic stabilization coming from Mott-Kondo volume collapse contributions. The model found partial support in the experiments of Tsvyashchenko *et al.* in 2010 [63], who measured the value of the electron field gradient in the α phase to be four times larger than the one in the γ phase.

Still there is no consensus about which is the best microscopic scenario that accounts for all available experimental observations regarding the α-γ phase transition. It could be that the complete explanation of the volume collapse would require ingredients from all of the approaches. To achieve a better understanding about the right mechanism behind the phase transition we clearly need to perform first-principles calculations using the most sophisticated and accurate methods at our disposal.

C. Previous *ab initio* studies

Within density functional theory, calculations of Ce in the local density approximation (LDA) and the semilocal generalized gradient approximation (GGA) were reported by various authors [2–5]. The observed experimental change in magnetic properties was reproduced in all calculations at the experimental lattice constants of the two phases. However, no signature of the volume collapse was found in the total energy versus volume curve. Based on the localization versus delocalization scenario of the phase transition, the failure of LDA and GGA was mainly attributed to the well known *self-interaction problem* intrinsic in these theories [73,74]. The self-interaction error has a tendency to delocalize electrons [75]. Local and semilocal approaches found a minimum in the cerium cohesive energy versus volume curve only corresponding to the α phase, whereas no stable solution was found for the γ phase (see Fig. 2 for results from this work; details of the calculations are given in Sec. IV). A recent study by Sakuma *et al.* [76] showed that even with the GW approach, experimental spectra for the γ phase could not be reproduced.

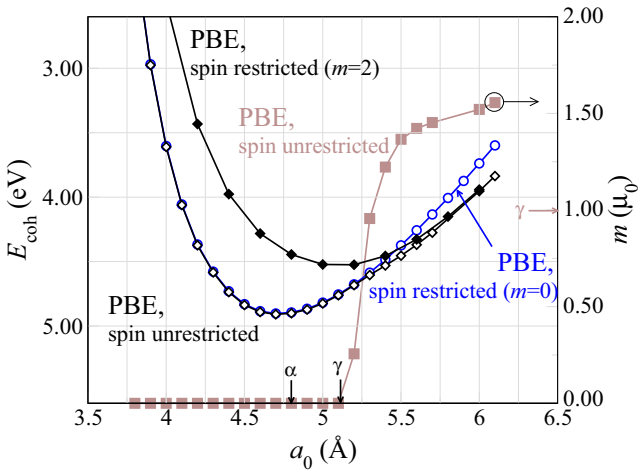

FIG. 2. Cohesive energy of cerium bulk within PBE spin unrestricted and restricted calculations. Experimental lattice parameters for the two phases at finite temperature [6] are marked by black arrows. The brown line represents the magnetic moment of the cerium atom of the unrestricted solution and refers to the scale on the right.

Following the failure of LDA and GGAs, a number of authors employed other methods. Usually it is assumed that the $4f$ electrons are localized in γ-Ce, and delocalized in α-Ce [3,17,24,77–83]. In particular, in 1995, Johansson *et al.* [17] obtained two cohesive energy versus volume curves in GGA calculations representing respectively the α and γ phases. In one case (α-Ce) $4f$ electrons were retained in the valence shell, while in the other case (γ-Ce) $4f$ electrons were frozen in the core.

The self-interaction-corrected local-spin-density approximation (SIC-LSD), was applied in the same spirit, and results consistent with the γ phase were obtained by Szotek *et al.* [77] and Svane [78]. The downside of the approach is that SIC-LSD can only capture the localized phase. So the authors relied on LSD (the spin polarized variant of LDA) to describe α-Ce. Combining total energy curves from the two theories produced a satisfactory estimation of the transition pressure. The difference between the two phases amounts to a few meV, as also observed in experiment. Lüders *et al.* [81] further extended the SIC-LSD study of cerium by incorporating temperature effects through entropic contributions, and obtained a slope of the phase transition line in the P-T phase diagram in agreement with the experimental one.

LDA+U calculations by Shick *et al.* [82] and Amadon *et al.* [24] also reproduced the physical properties of the γ phase, by accounting for the localization of the f electrons. They also predicted a magnetically polarized configuration of the system, in agreement with experimental results, and a lattice constant close to the one of γ-Ce. Interestingly, during the search of the ground state, the authors found multiple metastable energy minima in the total energy versus volume curve. We also found multiple stable solutions in our work, which will be discussed extensively in the remainder of the article. Wang *et al.* [83] extended the previous LDA+U studies. Following the SIC-LSD approach of Lüders *et al.*, they associated LDA and LDA+U results with the α and γ phases, respectively, and added an estimation of the entropic contributions to reproduce the cerium phase diagram.

LDA+DMFT approaches the problem from a different perspective. Also adding a localizing contribution for the f electrons to LDA, LDA+DMFT studies [51,84–90] aim to describe both phases within a single theory. The main result of LDA+DMFT is the prediction of an increased spectral weight at the Fermi level going from the γ to the α phase. As previously mentioned, the photoemission spectrum of cerium shows, in the low-volume phase, a typical three-peak structure, which several authors considered as the proof for the presence of Kondo physics [18,19,91] in the α-γ transition. SIC-LSD and LDA+U cannot reproduce this three-peak structure. The nature of the three peaks and its link to the Kondo physics has been, however, a matter of everlasting controversy. The three-peak structure appears both in the Hubbard model and in the Anderson impurity (or Kondo) model [40,42,66,67].

The solvers that usually enter the DMFT scheme introduce an electronic temperature. For the case of cerium, the temperatures usually reported were on the order of the critical temperature of the α-γ transition, or slightly lower. Low temperature calculations were hindered by the large computational requirements of low temperature quantum Monte Carlo calculations. As a consequence of this limitation, different authors reported different LDA+DMFT results. Held *et al.* [85] in 2001 reported a free energy curve with slightly negative curvature. This would be a signature of the phase transition, but in 2006 Amadon *et al.* [51], with a different implementation of the DMFT method, suggested that no negative curvature would emerge, even reaching temperatures below the ones reported in the previous study. Amadon *et al.* subsequently emphasized the role of entropy in the transition. Recently, Bieder *et al.* [92] performed calculations on fcc cerium with a more efficient implementation of DFT+DMFT. They were able to reach lower temperatures and to rule out the long lasting diatribe on the presence of the negative curvature. The latter appeared on the internal energy curve at temperatures compatible with the α-γ phase transition. However, the authors reported no evidence of the transition in the free energy curve at low temperature.

Lanatà *et al.* [93] approached the problem with a combination of DFT and the Gutzwiller approximation (LDA+GA), which can be viewed as a simplification of the LDA+DMFT approach with the possibility of exploring the zero temperature limit. The authors suggested a persistence of the phase transition at low temperature when spin-orbit coupling is included. The study was later extended to finite temperature by Tian *et al.* [94].

The persistence of the phase transition to zero temperature has been questioned [93,95]. Whether a double minimum exists or would only emerge in the free energy curve at finite temperature, due to entropic effects as suggested by Amadon *et al.* [51], is still a matter of debate. We showed previously [7] that at $T = 0$ K both phases are captured by employing hybrid functionals and exact exchange plus correlation in the random-phase approximation [8–10]. Similar results were obtained by Devaux *et al.* [96] with a different methodology. In our approach all electrons are considered, and, in contrast to LDA/GGA+U or LDA+DMFT studies, they are treated on the same quantum mechanical level.

IV. COMPUTATIONAL SCHEME: HYBRIDS AND THE RANDOM-PHASE APPROXIMATION

As the name suggests *hybrid functionals* combine the local/semilocal density functional approximation (DFA) for exchange and correlation (XC) with a fraction of exact exchange. In the simplest formulation, hybrid functionals are expressed as

$$E_{\rm xc}^{\rm hyb} = E_{\rm c}^{\rm DFA} + aE_{\rm x}^{\rm EX} + (1-a)E_{\rm x}^{\rm DFA}, \quad (1)$$

where correlation is retained at the level of semilocal DFA ($E_{\rm c}^{\rm DFA}$) and exchange is balanced between Hartree-Fock ($E_{\rm x}^{\rm EX}$) and standard XC functionals ($E_{\rm x}^{\rm DFA}$) through the parameter a. The latter depends on the employed Kohn-Sham (KS) functional and can be determined either by fitting to experimental data [97] and/or high-level quantum-chemistry results for molecules, or from considerations linked to the *adiabatic connection* (AC) formulation of the exact XC functional [9,98,99]. In 1996, Perdew, Ernzerhof, and Burke proposed to choose $a = 0.25$, considering atomization energies in fourth-order Møller-Plesset perturbation theory [100]. The performance of this formulation is, of course, related to the GGA functional in use, but it turned out that for the PBE functional $a = 0.25$ is actually a very good estimation. The functional, now termed PBE0 [101], became very popular and largely contributed to improved results for a wide range of systems [102]. Additional flexibility was introduced in hybrid functionals by partitioning the exchange term into short-range and long-range contributions. This led to *screened hybrid functionals*, of which one of the most prominent examples is HSE06 [10,103,104]. Hybrid functionals, containing a fraction of exact exchange, often handle localized states well, despite the fact that they are not rigorously self-interaction-free [105–107]. For this reason we decided to test them for the difficult case of the α-γ phase transition in cerium [108].

In Kohn-Sham calculations with (nearly) degenerate ground states, a finite electronic temperature is usually introduced to accelerate the convergence of the electronic minimizer [109–111]. In cerium, the remarkably large number of almost degenerate states near the Fermi energy requires a very high temperature, which introduces a large electronic entropy contribution. The ground state energy of the system is obtained from the free energy making use of a Taylor expansion [112,113]. Occupying all the almost-degenerate levels would require a very high broadening of the electronic level occupation, which would question the reliability of the extrapolation to the ground state. Another possible approach would be to manually set the occupation of the levels. However, this would bias the self-consistent field (SCF) cycle. Therefore, the calculations were started at a given bond distance with a high electronic temperature ($T^{\rm el} \approx 10\,000$ K, $k_B T^{\rm el} \approx 0.86$ eV), which was subsequently reduced. The initial broadening of the one-electron energy levels allows the valence electrons to populate all the low lying excited electronic states. In subsequent calculations for the same bond distance, the temperature is gradually reduced until the ground state is stabilized at $T^{\rm el} \approx 0$ K. This procedure facilitates an initial sampling of all almost degenerate configurations, and a final choice of only the most stable ones.

More than one stable solution is found in hybrid functional PBE0 and HSE06 calculations for cerium systems. The *multisolution* behavior is a known phenomenon when electronic configurations are close in energy [114]. This is often the case for open shell systems. Approaches that are based on the density matrix rather than the density are more susceptible to local minima in the potential-energy landscape of the electrons. If the orbital symmetry is broken the initialization of the system has a direct influence on the outcome of the SCF cycle: filled orbitals are energetically favored over empty ones, they are pushed down in energy, and it is energetically beneficial for the system to keep the initial orbital occupations. This is a known phenomenon in Hartree-Fock calculations [114] and is generally found in all approaches that create orbital polarization, such as DFT+U [82,115] and SIC-LSD [81]. It was reported [116] that also hybrid functionals exhibit this behavior. We will show in the remainder of this work that the presence of multisolutions in hybrid functionals turned out to be decisive for the study of the α-γ phase transition.

In our analysis the multisolution behavior arises as follows. Changing the distance between the atoms initializes the system in a different configuration at each bond length. As mentioned before, the Hartree-Fock exchange potential tends to preserve the given configuration. The sampling of the possible electronic states during the SCF cycle happens therefore not on all available states, but only on those configurations that are similar to the initial one. As a consequence, the system falls into several different solutions when scanning a range of distances. The different solutions are energetically stable, so we can restart calculations at neighboring distances with the previously computed electronic structures and generate full curves. This approach provides an assessment of multiple solutions but it does not guarantee, in general, that the real ground state of the system is reached.

To improve the accuracy of the calculations by incorporating correlation effects at a higher level of theory, we applied a postprocessing correction for exact exchange plus correlation in the random-phase approximation, (EX+cRPA)@(PBE/hybrids). The random-phase approximation was introduced already in the 1950s, in the context of the homogeneous electron gas. In a series of papers published by Bohm and Pines [117–120] it was suggested that a good estimation of correlation in the homogeneous electron gas could be obtained by separating the collective degrees of freedom from the single-particle degrees of freedom. This leads to an inclusion of the long-range Coulomb interaction in the collective behavior of the system, while the single-particle interaction is reduced to a short-range screened interaction. The RPA neglects the coupling between the collective and the single-particle degrees of freedom. In modern applications of RPA, a sum of all Feynman ring diagrams in the perturbative expansion of the correlation energy removes some divergence problems intrinsic to order-by-order expansions for homogeneous electron gas [121].

It can be shown [122] that the correlation energy within RPA can be computed from the charge susceptibility according to the expression

$$E_{\rm c}^{\rm RPA} = \frac{1}{2\pi}\int_0^\infty d\omega {\rm Tr}\{\ln[1-\chi^0(i\omega)v] + \chi^0(i\omega)v\}, \quad (2)$$

with v being the bare Coulomb interaction, $\mathrm{Tr} = \int d\mathbf{r}d\mathbf{r}'$, and $\chi^0(\mathbf{r},\mathbf{r}',i\omega)$ the independent-particle response function of the KS reference system:

$$\chi^0(\mathbf{r},\mathbf{r}',i\omega) = \sum_{ij} \frac{(f_i - f_j)\psi_i^*(\mathbf{r})\psi_j(\mathbf{r})\psi_j^*(\mathbf{r}')\psi_i(\mathbf{r}')}{\epsilon_i - \epsilon_j - i\omega}. \quad (3)$$

Here $\chi^0(\mathbf{r},\mathbf{r}',i\omega)$ is formulated in terms of the KS orbitals, with occupation numbers f_i. When applying EX+cRPA, the exact-exchange energy cancels the spurious self-interaction error present in the Hartree energy and the RPA correlation is fully nonlocal.

The success of the random-phase approximation in DFT has been demonstrated in a series of works on, e.g., molecular properties [123–126], periodic systems [127–129], and adsorption problems [130–133]. A major drawback of the RPA approach remains the high computational cost, which still hinders a widespread use. In this work, for example, RPA could be employed only for cluster systems. Moreover, RPA is generally implemented as a postprocessing correction, which makes the final result dependent on the starting point, i.e., on the functional that is employed. For instance, we will show in Sec. V B that (EX+cRPA)@PBE provides an outcome strongly influenced by the PBE input wave functions for the case of cerium. On the other hand several improvements beyond the RPA have been proposed recently, which make RPA-based methods an active field of research.

All calculations in this work were performed with the all-electron Fritz-Haber-Institut *ab initio* molecular simulations code (FHI-aims) [14,134] that is based on numeric atom-centered orbitals (NAO). Relativistic effects are treated at the level of the scaled zero-order regular approximation (ZORA) [135]. Here we present results obtained using the PBE0 hybrid functional [9] for both cluster and periodic systems [136] and show that the HSE06 hybrid functional [10] yields a similar description. For comparison we also applied the local density approximation in the parametrization of Perdew and Zunger [73] and the Perdew-Burke-Ernzerhof generalized gradient approximation (PBE) [101]. Periodic calculations were performed with one atom in the unit cell and a $6 \times 6 \times 6$ k mesh. The hybrid functional calculations were carried out with a tier 1 NAO basis [134,137] whereas for (EX+cRPA)@PBE/PBE0 it proved necessary to go up to tier 3. The sampling of the BZ and basis set that is used give us accurate total energies within 5 meV, which is sufficient for the energy scale of interest here. In general, ferromagnetic ordering is assumed in our spin-polarized calculations; see Ref. [138] for a discussion on the inclusion of disordered magnetic moments in the calculations.

V. RESULTS

A. Cerium bulk

The cohesive energy (E_{coh}) of cerium bulk obtained using different exchange correlation functionals (LDA, PBE, PBE0, and HSE06) is presented as a function of the lattice constant in Fig. 3. The experimental lattice constants of the α and γ phases of cerium, at 77 and 273 K, are also reported. The LDA and PBE results are in agreement with previous calculations [17,24,79,81,83] and exhibit only one minimum.

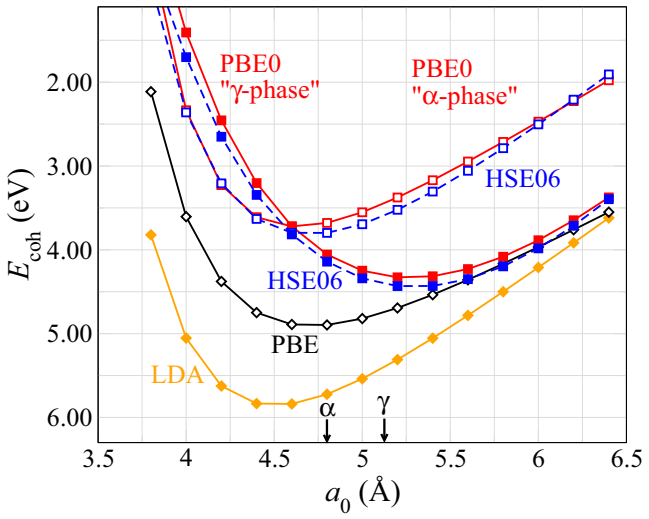

FIG. 3. Cohesive energy [$E_{\mathrm{coh}} = -(E - \sum E^{\mathrm{atom}})$] of cerium for spin unrestricted calculations as a function of the lattice constant (a_0). Dashed lines show HSE06 results. The spin moment increases with volume for the LDA and PBE solutions, while in PBE0 and HSE06 it remains approximately constant at zero and one-half for the α- and γ-like solutions, respectively. Experimental lattice parameters for the two phases at finite temperature [6] are marked by black arrows.

The associated volume is consistent with the α phase, although the actual value is underestimated. In contrast, in PBE0 and HSE06 two stable solutions are found. One solution has a minimum approximately coinciding with the LDA or PBE minimum, while the second reaches its equilibrium position at a much larger lattice constant, consistent with the one of the γ phase. The magnitude of the cohesive energy systematically reduces from LDA to PBE, and from PBE to PBE0. PBE0 and HSE06 results are almost identical, and will be considered as equivalent for the remainder of the article. In Table I the values for the equilibrium lattice constant, cohesive energy, bulk modulus, and magnetic moment are reported for bulk PBE and PBE0 calculations together with experimental reference values and previous calculations.

In LDA and PBE the system does not show a magnetic moment at the equilibrium lattice constant. A finite value for the spin only develops when the lattice constant is increased, see PBE results in Fig. 2, and eventually approaches the experimental value for the γ phase at the γ equilibrium lattice constant. A similar behavior is obtained with LDA. One should remember that the γ phase of cerium metal displays localized magnetic moments but does not assume ferromagnetic order. In this sense the spin component present in our calculations only approximates the real behavior of the system.

As shown in previous studies (see, e.g., Sec. III C), it is possible to produce two distinct PBE solutions by restricting the magnetic moment to the experimental values of the α and γ phases. The results of spin constrained PBE calculations are reported in Fig. 2. The spin unrestricted curve is the same as in Fig. 3. The brown curve represents the change of magnetic moment of the spin unrestricted solution with respect to the lattice constant. The abrupt emergence of a magnetic moment around the experimental lattice constant of the γ phase is representative of the observed change in

TABLE I. Comparison of the computed equilibrium lattice constants, bulk moduli, and cohesive energies for the α and γ phases with those of other calculations and experiments. In Ref. [17] LDA and GGA (Becke-Perdew gradient correction) calculations for the α and γ phases were modeled by retaining the f electrons in the valence shell (α phase) and the inert core (γ phase). In the SIC-LSD and LDA+U the α-phase results refer to LDA and LSD calculations.

	α-Ce			γ-Ce		
Method	a_0 (Å)	E_{coh} (eV)	B (GPa)	a_0 (Å)	E_{coh} (eV)	B (GPa)
LDA (this work)	4.50	5.84	64.1			
PBE (this work)	4.68	4.93	36.6			
PBE0 (this work)	4.63	3.76	50.5	5.22	4.35	28.3
LDA[a] (f in core for γ)	4.61		47.7	5.12		31.2
GGA[b] (f in core for γ)	4.80		39.1	5.30		28.8
SIC-LSD[b]	4.69		44.3	5.14		34
LDA+U[c]	4.52		59	5.04		34
Expt.[d]	4.83	4.3	27	5.16		19

[a]Reference [17].
[b]Reference [79].
[c]Reference [24].
[d]References [53,139,140].

magnetic properties along the α-γ phase transition and was already observed in earlier DFT studies [2]. A different curve can be generated by constraining the spin of the system. We took the extreme case in which both the magnetic moments of the $4f$ and the $5d$ electrons are aligned, $m = 2\ \mu_0$. In this configuration the system has an equilibrium lattice constant close to the experimental value for the γ phase. The two PBE solutions now have lattice constants and magnetic properties that are compatible with the experimental values for the α and γ phases, respectively. Eriksson *et al.*, however, already pointed out that this approach to describe both phases and the phase transition within LDA/GGA fails for the energy of the system [3]. Johansson *et al.* [17] managed to produce two different solutions in LDA or GGA calculations by freezing or unfreezing the f electrons in the core. Restricting the f electrons to the core is, in practice, similar to imposing a finite value of the spin to the system, because when spins are aligned the f-f intersite hybridization is negligible. However the authors had to apply an arbitrary shift to the curves in order to obtain a reasonable transition pressure. Also in the present calculations the energy of the solutions is an issue. With 0.5 eV, the energy difference is more than an order of magnitude larger than what has been measured in experiment.

The band structure of the PBE spin unrestricted and restricted solutions is presented in Fig. 4 along the main directions through the Brillouin zone of the fcc structure. The bands are plotted for the equilibrium lattice constants of 4.6 and 5.2 Å, respectively. Only the spin up component of the bands is reported. In PBE spin unrestricted calculations the magnetic moment at the equilibrium position is zero, so the spin up and down bands are equivalent. For spin restricted calculations the spin down bands correspond to a rigid upward shift of the spin up bands and are therefore omitted from the discussion.

The comparison between the two sets of bands shows the similarities between the two types of calculations. In both cases the two bands below the Fermi level, of mixed d and f

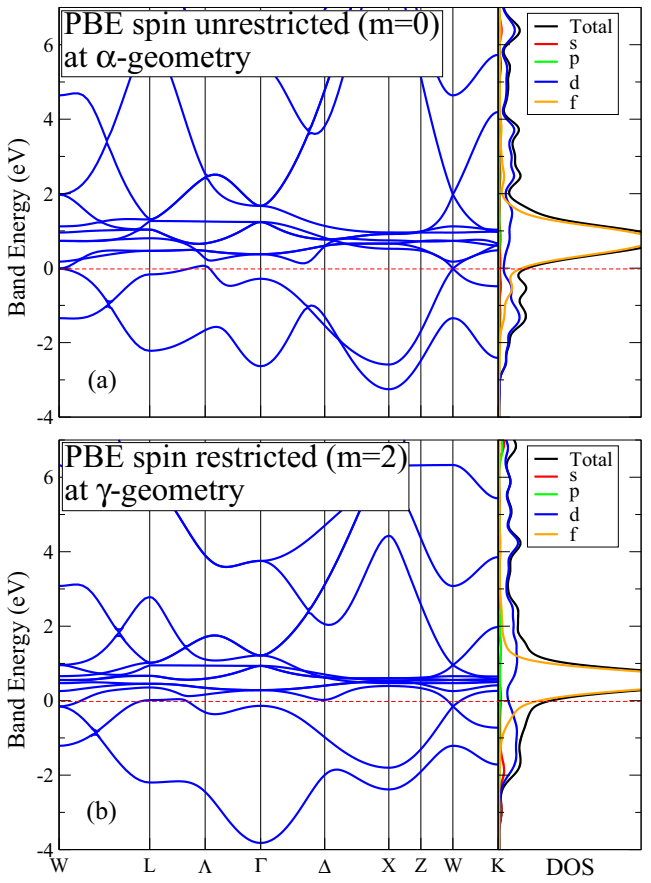

FIG. 4. PBE band structure for spin unrestricted (a) and restricted (b) calculations. The band structure refers to the spin up component and it is taken at 4.6 Å in (a) and 5.2 Å in (b). For spin unrestricted calculations the spin up and down bands are equivalent. For spin restricted calculations the spin down bands correspond to a rigid upward shift of the spin up bands. The energy zero is the Fermi energy. The DOS is reported in the right panel.

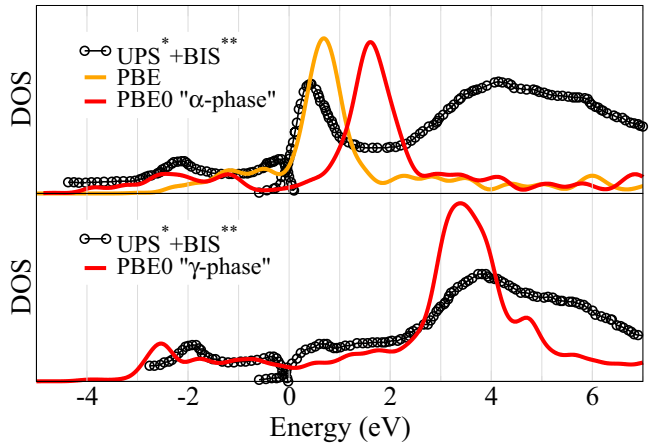

FIG. 5. Density of Kohn-Sham states of the α- and γ-like solutions of Fig. 3. Zero is the Fermi energy. Direct (*) and inverse (**) photoemission experiments are taken from Refs. [37,47], respectively.

character, show a large dispersion, and they strongly hybridize around the X point and along the Δ and Z directions. At and above the Fermi level lie a number of dispersionless f bands. Their bandwidth is smaller in restricted calculations, but this is also observed for unrestricted calculations by increasing the lattice constant. The overall agreement with previously computed band structures [81,141,142] is good.

Now we discuss the results from hybrid functional calculations. The two PBE0 solutions differ in their electronic structure as reflected in the density of states, shown in Fig. 5, and the magnetic moment of the cerium atom (m); see Sec. VI A. The magnetic moment of the low volume phase lies around 0.2 μ_0, while in the high volume phase m is close to one. Also the number of f electrons is approximately one in both phases, in agreement with positron annihilation experiments; see Sec. III A.

The density of states (DOS) is plotted in Fig. 5 at the equilibrium distances of the two phases. The DOS for negative energies corresponds to occupied levels, zero corresponds to the Fermi energy (E_F), and the empty states are found at positive energies. The reported DOS is the sum of the spin up and spin down DOS. The PBE DOS, together with direct and inverse photoemission data, are also shown for comparison. To simplify the notation, the two hybrid functional solutions will be labeled with the letters "α" and "γ" in the remainder of this article. This is related to the similarity of the two PBE0 solutions with the two experimental phases of cerium, reflected in, e.g., the equilibrium lattice constant, magnetic moment, and KS DOS. The PBE0 γ phase displays some peaks below the Fermi energy, of which the peak around -3 eV arises mainly from an f contribution and the others accommodate d electrons. The region of the empty states is instead dominated by a major peak between 3 and 4 eV. The α-like phase is characterized by a strong peak between 1 and 2 eV. PBE reproduces the experimental central peak. Going from PBE to the PBE0 α-phase solution, the spectral weight is shifted away from E_F: the occupied orbitals are moved to lower energy, the empty ones to higher energy.

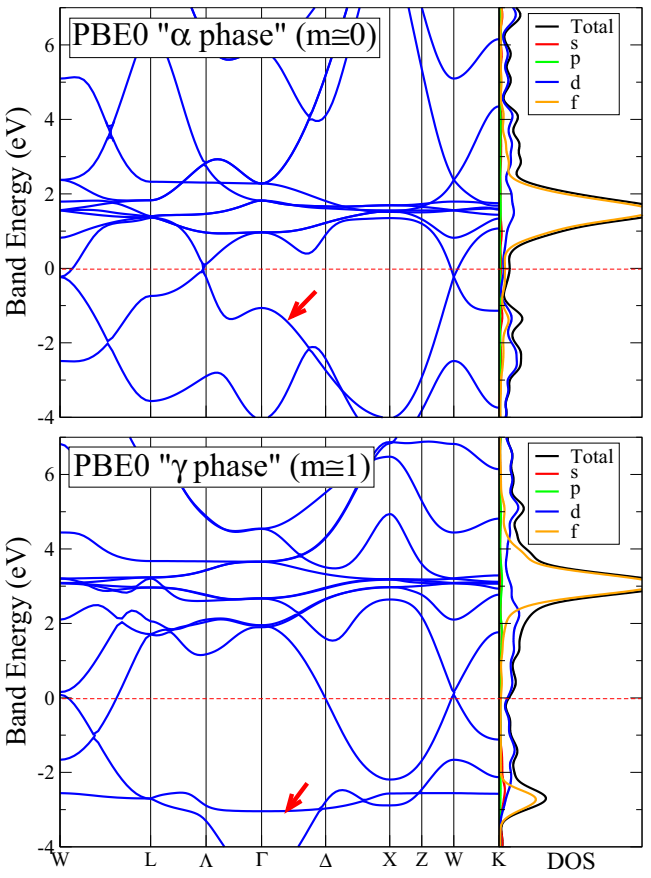

FIG. 6. PBE0 band structure for the α and γ solutions. The band structure refers to the spin up component and it is taken at 4.6 in α and 5.3 Å in γ. The spin down bands of the α phase are like the spin up bands, but shifted up by a small amount. The spin down bands for the γ phase are similar to the spin up ones, but the flat f band is shifted to around 4 eV above E_F. The energy zero is the Fermi energy. Red arrows indicate the band that becomes dispersionless and occupied in γ. The DOS is also reported on the right panel.

As already pointed out, the experimental spectrum of the α phase has been a matter of controversy for a long time. In particular, the characteristic three-peak structure has been observed in all measurements, but the nature of the peaks, if they are of an f nature or not, remains uncertain [42]. Moreover, in cerium the surface contributions play an important role and the surface is believed to preserve γ-like features also in the α phase. Consequently, the peak at around 4 eV could belong to the γ-like surface. It is therefore not certain whether the PBE and PBE0 α-like densities of states are missing some features, as suggested by LDA+DMFT studies [51,84–86,90], or whether they describe the cerium spectra as they would be if measured at 0 K without surface effects.

In this regard, we note that DFT calculations can properly address the ground state of the system even if the Kohn-Sham spectrum does not agree with the photoemission spectrum either in peak intensities or in peak positions.

The band structure of the PBE0 solutions is reported in Fig. 6. Only the spin up component is shown. The spin down bands of the α-phase solution are like the spin up bands, but shifted up by a small amount. In the α phase the two occupied

bands hybridize strongly around the X point and along the Δ and Z directions, similar to what was observed in PBE, while the unoccupied f bands are moved to higher energies by around 1 eV with respect to PBE. In the PBE0 γ phase the nearly dispersionless empty f bands are shifted up by around 3 eV with respect to PBE. Furthermore, major differences are observed for the occupied states. A flat band of f character is occupied at around 3 eV below E_F. The spin down bands for the γ phase are similar to the spin up ones, but the flat f band is shifted to around 4 eV above E_F. The band indicated by the red arrows in Fig. 6 becomes nearly dispersionless and fully populated going from the α to the γ phase. A $4f$ peak in the DOS appears for the occupied states in correspondence with the flat band. This feature is also observed in the SIC-LSD calculations of Lüders *et al.* [81]. It emerges in correspondence with the appearance of a magnetic moment close to one in the γ phase, and can be associated with the localization of one $4f$ electron when going from the α to the γ PBE0 solution.

The f electron localization process in hybrid functionals can be visualized in a more pictorial way by plotting the difference between the electron density of the PBE0 α- and the γ-like solutions, $n_\alpha(\mathbf{r}) - n_\gamma(\mathbf{r})$, shown in Fig. 7. A slice of the density difference is shown in Fig. 7(a), corresponding to the [100] plane, or equivalently to the [010] and [001] planes, at the lattice constant of 4.6 Å, where the two solutions have almost equal cohesive energy. The green sphere marks the Ce atom in the unit cell. Blue and red colors indicate a surplus of electron density in the α and γ phases, respectively. The plot shows that the interstitial region between the cerium atoms in the periodic environment is colored blue, while the red color resides mainly on lobes around the atomic sites. This reveals that the α-like phase has a higher density in the interstitial region with respect to the γ-phase solution. Thus, the degree of electron localization/delocalization in the two phases is significantly different. A comparable effect, but much weaker, arises if the analysis is performed between the spin unrestricted and restricted PBE calculations (not shown).

By plotting a three-dimensional isosurface with a cutoff at negative values of the density difference (i.e., where the γ-like phase has a larger number of electrons with respect to the α-like phase) one obtains a surface with the shape of an f orbital of xyz or $z(x^2 - y^2)$ symmetry, Fig. 7(a). This provides a strong indication that the delocalized electrons in the interstitial region are actually $4f$ in nature, and that it is the balance between localization and delocalization of the f electrons that plays a key role in the emergence of the double minimum in the cohesive energy curve. We will show in the next section that the different magnetic moment of the two phases stabilizes an underlying difference in the electron wave functions. This observation supports the picture that the driving mechanism of the α-γ phase transition is linked to a change in the behavior of the $4f$ electrons. The f states would participate in the bonding in α-Ce, and they would not in γ-Ce. This is also what was assumed in previous calculations on cerium by means of SIC-LSD and LDA+U. In our study, however, it appears not as an *a priori* constraint of the system, but it arises naturally from calculations in which all electrons have been treated on the same quantum mechanical level.

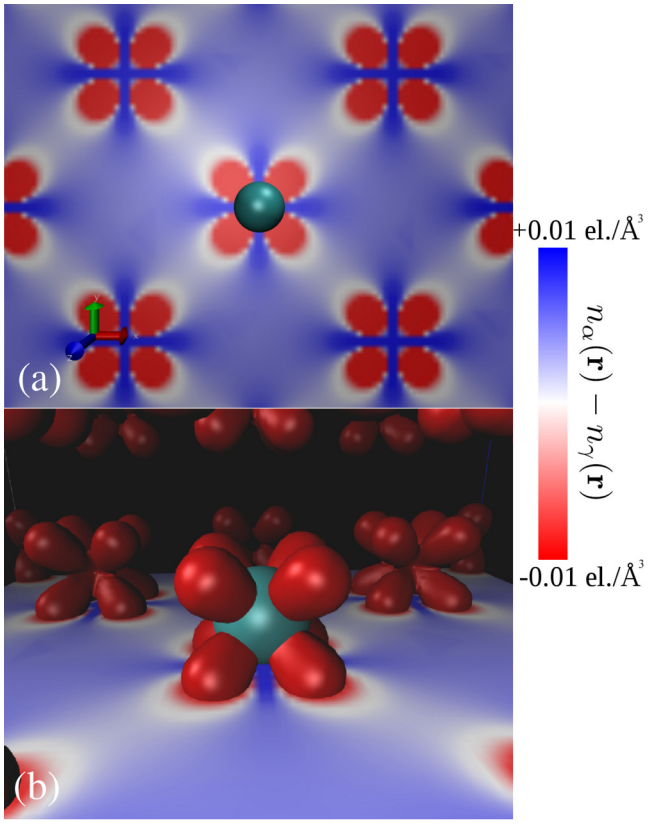

FIG. 7. Difference between the PBE0 bulk electron densities of the α and γ phases at the same lattice constant of 4.6 Å, at which both phases have the same energy. The green sphere marks the position of a Ce atom. (a) The density difference is projected onto the [100] plane; the [010] and [001] planes are equivalent. The α phase has a larger contribution in the interstitial region, whereas the γ phase density is more localized around the nuclei. (b) Isosurface with negative cutoff on the density difference. The isosurface resembles an f orbital of xyz, $z(x^2 - y^2)$ symmetry. The projection onto the [100] plane is also reported.

It proved useful to perform PBE0 spin unpolarized calculations to further analyze the hybrid functional results. In Fig. 8 the curves of Fig. 3 are reported along with spin unpolarized PBE0 calculations.

At 5.4 Å the electronic structure between the direct and the restarted calculations differs. The direct solution, which has been approached from the left (i.e., smaller lattice constants), resembles that of the equilibrium lattice constant. The restarted calculation, on the other hand, has been approached from the right and carries the signatures of the electronic structure at larger lattice constants. The behavior of the system changes with the smooth rearrangements of the f states. The electronic structure of the underlying s, p, and d states is very similar in both situations, but the f states can be accommodated in different ways. This is seen in the band structure of the two PBE0 unpolarized solutions; see Fig. 9. The two sets of bands are similar, but some differences are present in the f bands above the Fermi energy. The empty f states are shifted to higher energy by around 1 eV in the restarted solution. The band that is flat and fully occupied in the PBE0 γ phase does not show the same properties for unpolarized calculations.

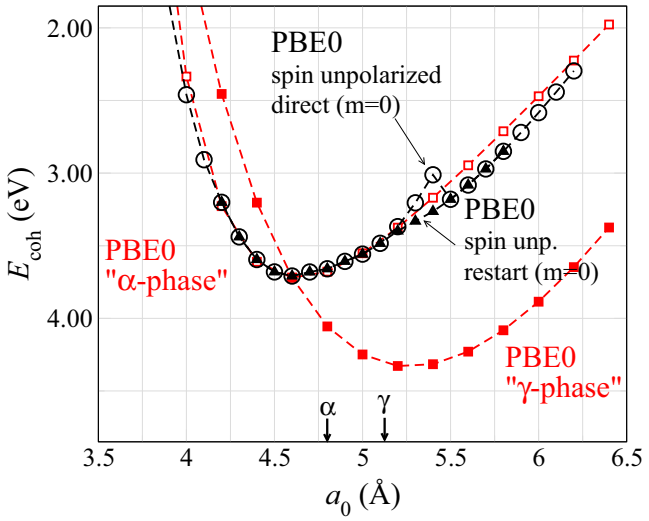

FIG. 8. PBE0 cohesive energy curves for the spin polarized (red) and unpolarized (back) solutions.

However, we will show next that trademarks of the γ phase are present in the unpolarized restarted calculations.

Figure 10 exemplifies the differences between the two PBE0 spin unpolarized solutions. In the first row of Fig. 10 the density difference between unpolarized calculations is displayed for a volume slice, parallel to the [100] plane, that is approaching the cerium atom, green sphere, from behind. The volume slice is moved, going from left to right, from the center of the f-shaped lobes to a position closer to the atom. Similarly, in the second row the difference is taken, at the same lattice constant and steps for the volume slice, between the direct unpolarized solution and the ferromagnetic γ-like PBE0 solution of Fig. 8. In the top right figure the density difference between the two unpolarized solutions displays similar features to the bottom right figure and to the spin polarized density difference of Fig. 7. It also shares with the spin polarized PBE0 results the same three-dimensional

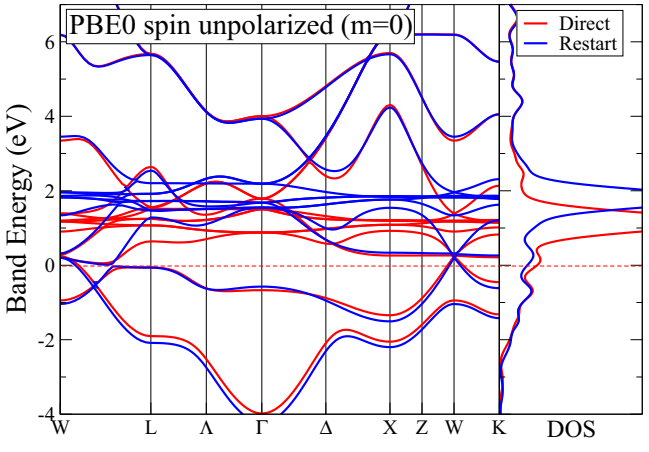

FIG. 9. PBE0 band structure for spin unpolarized (red) and spin unpolarized restart (blue) calculations. The band structure is taken at 5.4 Å. Zero is the Fermi energy. The DOS is also reported in the right panel.

f-shaped isosurface for negative values of the cutoff (not shown here). This reflects a wave function change when going from one spin unpolarized solution to the other, and proves that there is no need for a magnetic moment change to obtain two PBE0 solutions with distinct electronic structures, as also evidenced by Devaux *et al.* [96].

In Fig. 10, going from left to right the volume slice approaches the atomic centers from behind. On can note that the red lobes have reduced spatial extension in the second row. The magnetic moment greatly favors localization of the f states in the γ phase, and the red regions collapse towards the atomic centers. The magnetic degrees of freedom help to stabilize the solutions that are already inherent in spin unpolarized calculations. This is a significant difference from PBE calculations for Ce, where it is not possible to obtain two different solutions with the same magnetic moment.

The top left panel provides additional insight into the results. It makes clear that the spatial arrangement of the electrons in the two PBE0 spin unpolarized configurations, f electrons according to the isosurfece plots, follows a different symmetry. A discrimination between localization and delocalization becomes more difficult and it is instead more interesting to focus on the change in the preferred directions along which the f electrons are arranged. Unfortunately, it is not possible to address the symmetry lowering, going from the γ to the α phase, suggested by Nikolaev and Michel [61] due to the too small dimension of the unit cell. Nevertheless, we acknowledge a symmetry breaking going from one phase to the other.

B. Cerium clusters

We considered cerium clusters to perform higher level calculations. We computed cerium clusters of increasing size with the PBE and PBE0 functionals, and EX+cRPA corrections. The clusters were cut from the face-centered cubic crystal structure, which characterizes both α and γ phases, in order to mimic the periodic environment. They were built with one atom in the center surrounded by shells of first, second, and third nearest neighbors. This procedure leads to configurations of thirteen, nineteen, and forty-three atom clusters as illustrated in Fig. 11. The fcc structure and the configuration with one atom in the central position were preferred over other possible ones, for instance the one cut from the fcc structure with a first tetrahedral shell and a total of fourteen atoms, in order to recreate the best bulk environment for the central atom.

In order to reduce edge effects the following expression for the effective cohesive energy of the clusters was used [143,144]:

$$E_{\rm coh} = -\left[E - \sum_{c=1}^{12}\left(N_c E_c^{\rm atom}\right)\right]\left(\sum_{c=1}^{12} N_c\sqrt{\frac{c}{12}}\right)^{-1}, \qquad (4)$$

where E is the total energy, N_c the number of atoms in the cluster with c nearest neighbors, and $E_c^{\rm atom}$ the atomic total energy for a c-fold-coordinated atom [145]. The formula assigns a weight, the second term in Eq. (4), to each atom depending on the number of nearest neighbors [146]. Atoms that are in the inner region of the cluster are more important. The central atom for instance, for which the shell of first nearest

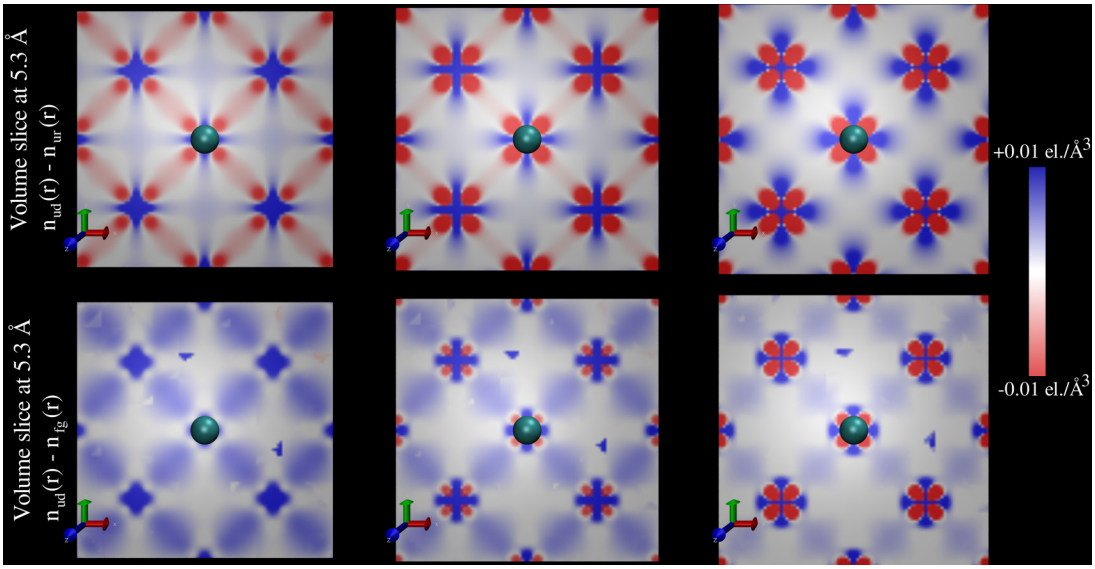

FIG. 10. Volume slices, parallel to the [100] plane, at a lattice constant of 5.3 Å of the density difference between direct (ud) and restarted (ur) spin unpolarized solutions (upper panels), and direct spin unpolarized (ud) and γ-like spin polarized (fg) solutions (lower panels). Going from left to right the volume slice is approaching the cerium atom from behind: in the first column the slice is placed at 0.6 Å behind the atom position, in the second column 0.5 Å, and in the third column 0.4 Å.

neighbors is complete, has weight one. All other atoms have a weight smaller than one.

We decided to perform unrestricted spin polarized calculations, which means that the system has no constraint on the total spin value. This approach guarantees that the system relaxes into one of the lowest, if not the lowest, states, with the corresponding optimal spin configuration. The outcome for the cohesive energy is reported in Fig. 12. The energy is plotted with respect to the lattice constant (a_0) in an fcc environment that would correspond to the distance between the atoms in the cluster.

All three clusters show similar features. The PBE functional gives a smooth curve for the cohesive energy. The magnetic moment of the central atom is zero around the equilibrium position and increases with increasing lattice constant [147]. PBE0 results instead give two stable configurations. They both lie at higher energies compared to the PBE curve and they are separated by approximately 1 eV. Curve (a) is stable at a lattice constant that is close to the PBE one and has the same magnetic properties. At the equilibrium position the spin value of solution (a) is almost zero. The minimum of solution (b) is found at a larger distance, and the spin of the central atom approaches one half [148].

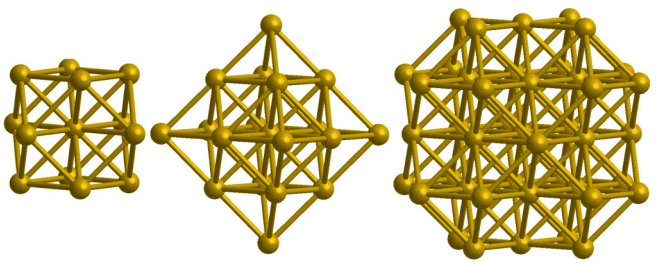

FIG. 11. Cerium clusters cut from the fcc crystal structure with a total number of 13, 19, and 43 atoms, going from left to right.

An analysis of the PBE and PBE0 solutions reveals that the different functionals preserve specific characteristics of the electronic structure in all clusters. The density of Kohn-Sham states projected onto the central atom is plotted in Fig. 13 for all clusters. The DOS in the plots is the sum of the spin up and spin down DOS. A Gaussian smearing of 0.2 eV is applied to the KS-DOS to facilitate readability. For PBE0, all states below -4 eV are identical in both solutions.

A characteristic that emerges from Fig. 13 is the presence of a prominent peak in the unoccupied states. A comparison with photoemission experiments for bulk cerium was reported in Sec. V A. For all cluster sizes, the peak of PBE and the PBE0 (a) solution lies between 1 and 2 eV whereas in solution (b) it is moved to around 4 eV. In both cases it arises from the $4f$ states.

In both PBE and PBE0 the similarities between Ce_{19} and Ce_{43} are remarkable. The spectra are dominated by the d and f states. In PBE and the PBE0 (a) solution the $5d$ levels have peaks mainly around -2 and -3 eV and just above the Fermi energy. In the PBE0 (b) solution the $5d$ states, occupied and empty, are close to E_F. The position of the occupied and empty $4f$ states is similar between the PBE and PBE0 (a) solutions, where the empty $4f$ states are close to E_F. In PBE0 (b) instead, the empty states lie at higher energies around 4 eV. A closer look around the Fermi energy reveals that there is a removal of f spectral weight from E_F going from PBE, PBE0 (a) to PBE0 (b). The f levels are pushed away from the Fermi level, while the occupied and empty d states come closer. The change in electronic structure arises therefore from the interplay (hybridization) between the $5d$ and $4f$ states.

Now, we address the impact of including correlation effects at the RPA level, as introduced in Sec. IV. We first discuss (EX+cRPA)@PBE results. The (EX+cRPA)@PBE cohesive

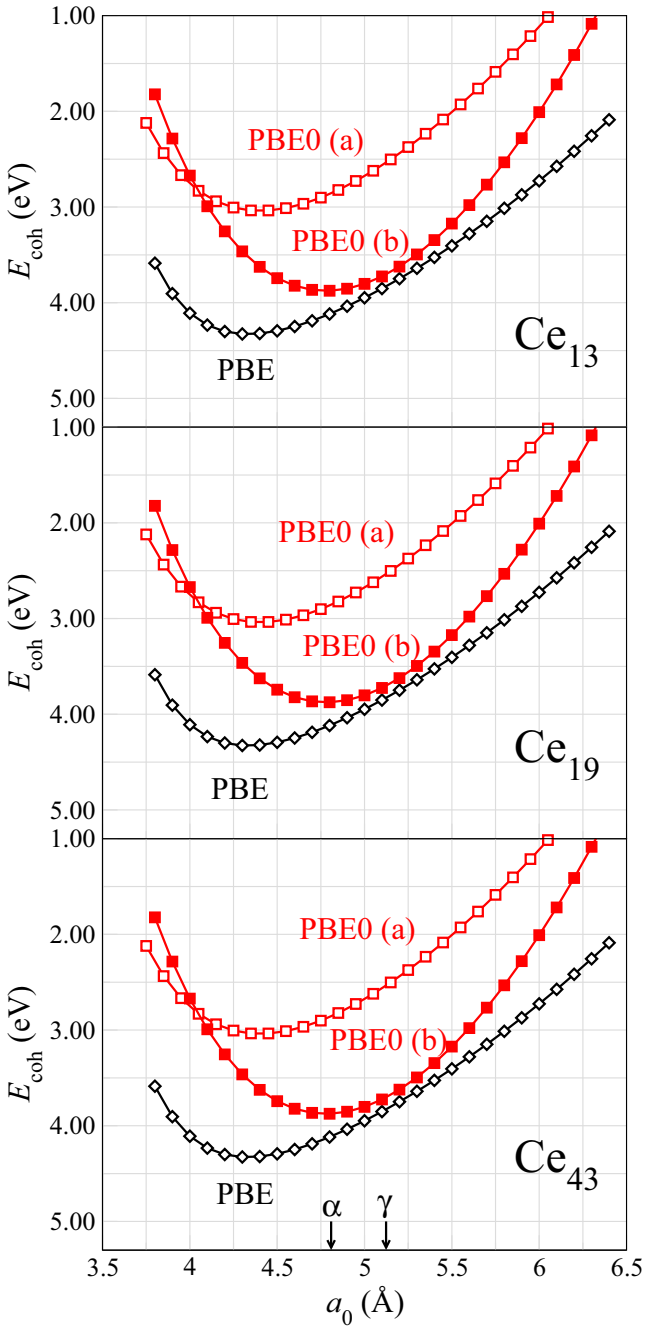

FIG. 12. PBE and PBE0 cohesive energy for the cerium clusters. a_0 is the lattice constant in an fcc environment that would correspond to the distance between the atoms in the cluster. (a) and (b) label the two configurations found within PBE0. Arrows on the energy axes: experimental cohesive energy from Ref. [140].

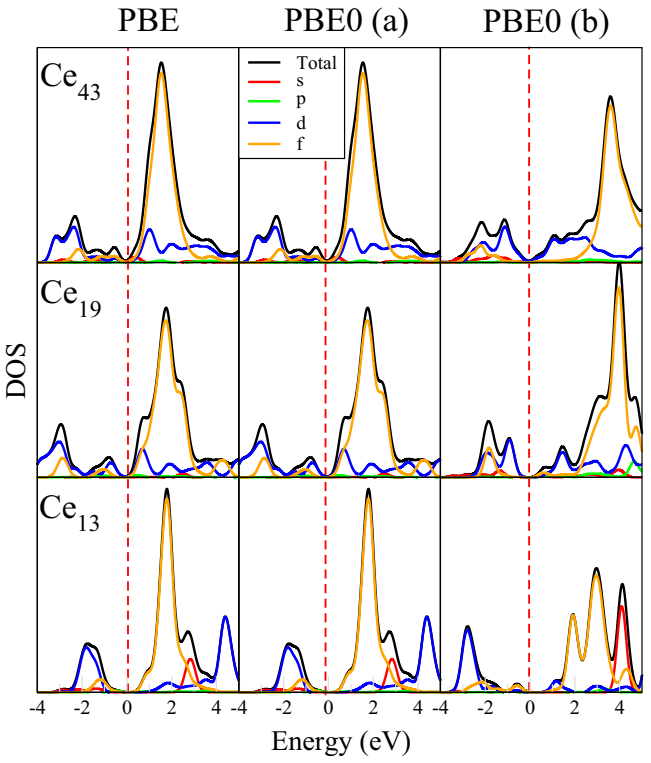

FIG. 13. PBE and PBE0 density of Kohn-Sham states (sum of spin up and down DOS). (a) and (b) label the two PBE0 solutions. The DOS is calculated at the equilibrium distances. The different colors label total (black), s (red), p (green), d (blue), and f (orange) DOS.

energy of Ce_{19} is reported in Fig. 14. Due to the computational cost of RPA the nineteen-atom cluster is the largest that could be studied with high level quantum many body techniques.

For both spin unpolarized and spin unrestricted PBE calculations the EX+cRPA correction causes a shift by around 2.5 eV to lower energies. On the other hand the equilibrium lattice constants are close to the PBE values: 4.35 and 4.30 Å for the PBE and (EX+cRPA)@PBE spin unpolarized results, respectively, and 4.40 and 4.26 Å for spin unrestricted results.

In the same figure the magnetic moment of spin unrestricted calculation is also plotted along with its $4f$ component. The spin component of the system is mainly dictated by the f

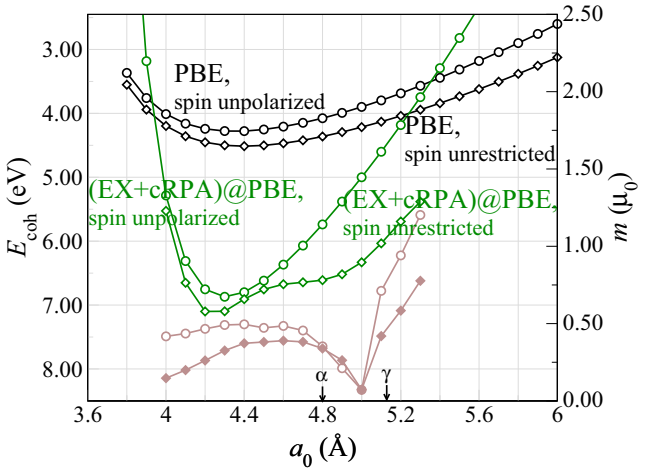

FIG. 14. PBE (black) and (EX+cRPA)@PBE (green) cohesive energy for the 19-atom fcc-cerium cluster as a function of the lattice constant. Both the spin unrestricted and the spin unpolarized configurations are reported. The total magnetic moment on the central atom (brown curve, open circles) and the $4f$ contribution to the magnetic moment (brown curve, filled diamonds) is shown for the spin unrestricted data and refers to the axes on the right.

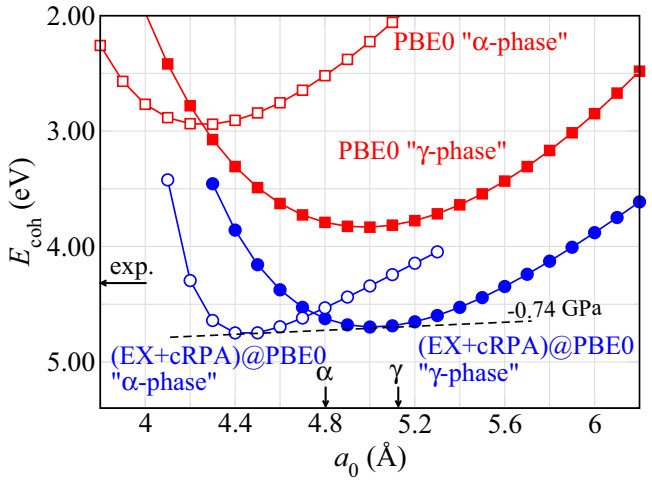

FIG. 15. Calculated (EX+cRPA)@PBE0 cohesive energy for the 19-atom fcc-cerium cluster as a function of the lattice constant. The dashed line illustrates the Gibbs construction for the transition pressure in good agreement with the extrapolated experimental $P_t \simeq -0.8$ GPa [52]. Arrows on the energy axes: experimental cohesive energy from Ref. [140].

electrons. For spin unpolarized calculations the EX+cRPA cohesive energy displays a smooth behavior with distance. Instead, (EX+cRPA)@PBE for the spin unrestricted results displays a region of negative curvature in correspondence with a change in the magnetic properties.

Ce_{19} is representative of the other clusters; see, e.g., the density of KS states in Fig. 13. However, the magnetic moment obtained with PBE for Ce_{19} is not representative of the PBE bulk results reported in Sec. V A. One could associate the two minima in the spin unrestricted results with the α and γ phases of cerium; however caution should be used. The absence of a double minimum or kink in the spin unpolarized (EX+cRPA)@PBE indicates that a wave function change is not captured either by PBE or by the EX+cRPA correction. The structure in the spin polarized (EX+cRPA)@PBE curve therefore arises from the magnetic moment of PBE, which assumes values far from the experimental ones. Combined with the largely overestimated binding energy, these features suggest that PBE is not a good starting point for higher level correlated methods for cerium even if it is able to capture some aspects of the phase transition. In the next paragraphs we will show that PBE0 is in effect better suited.

The (EX+cRPA)@PBE0 cohesive energy for Ce_{19} is reported in Fig. 15. The γ-like (EX+cRPA)@PBE0 solution is moved down in energy with respect to PBE0 by 0.8 eV, while the α-like solution lowers by as much as 1.8 eV. The energy shifts are linked to the KS density of states reported in Fig. 13. The low volume phase is shifted more in energy because the number of states near the Fermi level is higher in the α phase with respect to the γ phase. The higher density of states near E_F gives rise to a higher polarizability, with a subsequent increase in the RPA energy. More generally, the energy shift is related to the improved description of screening effects in RPA. The α phase is more affected by the cRPA correction as the screening is higher for delocalized electrons [149].

It will be explained in Sec. VI A that Ce_{19} is representative of the PBE0 bulk result. It is therefore one of the main achievements of this work that EX+cRPA reverts the energetic ordering of the two PBE0 solutions, and brings the difference in energy between the PBE0 α and γ phases in agreement with experiment. According to the extrapolation of the experimental data to zero temperature [51,52], the difference in internal energy (ΔU) between the two phases should lie between 20 and 30 meV, while the difference in cohesive energy for Ce_{19} amounts to $\Delta U \simeq 45$ meV within (EX+cRPA)@PBE0. The cohesive energy is a good estimate of the internal energy of a system at zero temperature if we neglect the zero-point motion of the atoms (which in fact should be negligible for heavy elements). The difference in cohesive energy is comparable to the experimental findings, even if it is larger than the experimental estimation of the maximum energy difference between the two phases. This leaves room for the estimated entropy contribution [51,52], $T\Delta S$, to play a role in the phase transition. The calculated lattice constants for the α- and γ-like phases are 4.45 and 5.03 Å, respectively. In other words, the lattice constant of the α phase is underestimated (4.83 Å at 77 K), but the agreement with the experimental value for the γ phase is good (5.16 Å at room temperature). Consequently, the estimated volume collapse is $\simeq$30% at zero temperature, instead of the 15% observed experimentally at ambient conditions [6]. The common tangent to the (EX+cRPA)@PBE0 cohesive energy curves leads, through the Gibbs construction, to a transition pressure of $P_t \simeq -0.74$ GPa at zero temperature. This is in good agreement with the extrapolated experimental $P_t \simeq -0.8$ GPa.

VI. PHASE DIAGRAM FOR THE α-γ TRANSITION

Hybrid functional calculations for cerium provide a new perspective for DFT methods in the description of the α-γ phase transition. In both PBE0 and HSE06 two solutions are found for clusters and the bulk. The double well observed in the cohesive energy versus volume curve shows the occurrence of a $T = 0$ K phase transition accompanied by a volume collapse that has not been obtained before in *ab initio* calculations. The two solutions display specific characteristics of the α and γ phases, including a good description of the change in magnetic and structural properties associated with the volume collapse. They also support the already suggested localization-delocalization process as a mechanism for the phase transition. However, the relative energetic order differs from what is expected according to the extrapolated experimental phase diagram at zero temperature.

Exemplified by the case of the nineteen-atom cluster, we showed that the EX+cRPA correction to hybrid functionals brings the two solutions close in energy and recovers the right energetic order of the two solutions. This provides agreement between the calculated transition pressure and the experimental data extrapolated to zero temperature. A similar result could be achieved by varying the amount of exact exchange included in the hybrid functional [150]. However, no adjustable parameters are involved in our calculations, and we rely only on a higher level description of exchange and correlation. In this section we will show that by adding entropic contributions to the cluster results (at the time of this study,

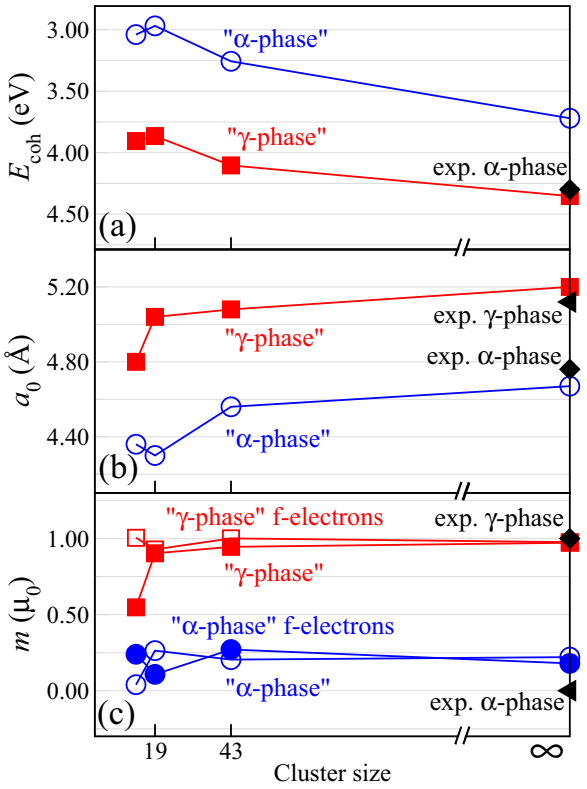

FIG. 16. PBE0 results for cerium clusters and corresponding bulk values for (a) the cohesive energy E_{coh}, (b) atomic distance corresponding to the lattice constant a_0 in the periodic environment, and (c) the magnetic moment on the central atom m. All clusters exhibit two solutions that converge to the calculated bulk limit. Experimental results marked on the right axis are taken from Refs. [6,140].

a periodic implementation of RPA was not available in the FHI-aims code) the temperature-pressure phase diagram of cerium can be reproduced qualitatively.

A. Towards the bulk

Looking at the electronic properties of the clusters, as reflected in the density of states of the central atom, we noted in Sec. V B that cerium clusters cut from the fcc crystal structure capture the essential physics of bulk cerium. The PBE DOS of the central atom converges to the PBE bulk DOS with increasing cluster size (from the comparison of Figs. 5 and 13). The same happens in PBE0, where the two phases maintain their distinctive features for all clusters, and the cluster DOS projected on the central atom is representative of the bulk DOS (from the comparison of Figs. 5 and 13). From Fig. 16 it becomes clear that there is indeed a trend in the physical observables of the two solutions when increasing the dimension of the system.

Figure 16 reports the values of the cohesive energy, the equilibrium lattice constant, and the magnetic moment (on the central atom) for all clusters and the bulk. Experimental data are also included for comparison. All properties approach the bulk limit with increasing cluster size. The two solutions for the bulk are in agreement with the experimental lattice constant and magnetic moments of the α and γ phases. It is also evident, from Fig. 16(c), that the spin component of the system mainly arises from the f electrons. It can be stated that PBE0 captures the essential physics of the two bulk phases for Ce_{19}, and that, as a consequence, (EX+cRPA)@PBE0 results for Ce_{19} would be representative of the periodic system. Therefore, it is reasonable to base our finite temperature analysis of the phase transition on the (EX+cRPA)@PBE0 calculations for Ce_{19}. The result is presented in the next section.

B. Finite temperature

In Sec. V B a pressure induced phase transition at zero temperature was related to the (EX+cRPA)@PBE0 calculations for the nineteen-atom cluster. Here we extend the results to finite temperatures by adding entropic effects to the ground state energy [5,17,79,81,83]. The first entropic contribution is configurational entropy. This is based on the assumption that the phase that is metastable at a given volume and pressure may become thermally populated as temperature is increased. We therefore adopt a "pseudoalloy" model for the transition [17], where the α and γ phases coexist with concentrations x^α and x^γ but do not interact [151].

In order to obtain a description of the system at finite temperature the Helmholtz free energy

$$F(V,T) = U(V) - TS \tag{5}$$

is required, where U is the internal energy, T the temperature, V the volume of the unit cell, and S the entropy. The free energy can be obtained from the partition function [83], which is an additive quantity for all the noninteracting components of the system, for which the following relation holds:

$$Z = e^{-\beta F(V,T)} = \sum_\sigma Z^\sigma = \sum_\sigma e^{-\beta F^\sigma(V,T)}, \tag{6}$$

where $\beta = 1/(k_B T)$, k_B is the Boltzmann constant, $\sigma = \{\alpha,\gamma\}$, and F^σ is the free energy of the α or γ phase. One can now define two quantities

$$x^\sigma = \frac{Z_\sigma}{Z} \tag{7}$$

in order to rewrite the free energy as

$$\begin{aligned} F(V,T,x^\sigma) &= -k_B T \ln Z \\ &= \sum_\sigma x^\sigma F^\sigma + k_B T \sum_\sigma x^\sigma \ln x^\sigma \\ &= \sum_\sigma x^\sigma F^\sigma - T S_{\text{conf}}. \end{aligned} \tag{8}$$

The quantity x^σ represents the contribution of one or the other phase to a determined state of the system and $S_{\text{conf}} = -\sum_\sigma x^\sigma \ln x^\sigma$ is the entropic contribution that arises from the coexistence of the two phases.

The free energy of a single phase can then be computed from

$$F^\sigma(V,T) = U^\sigma(V) - T\left(S^\sigma_{\text{el}} + S^\sigma_{\text{mag}} + S^\sigma_{\text{vib}}\right), \tag{9}$$

where U^σ is the internal energy, S^σ_{el} is the entropy arising from electronic degrees of freedom, S^σ_{mag} is the entropic contribution of the magnetic moment at each cerium site,

and $S^{\sigma}_{\rm vib}$ is the entropy associated with lattice vibrations. The (EX+cRPA)@PBE0 calculations reported in Sec. V B proved to be a reasonable estimation of the two contributions U^{α} and U^{γ} according to the extrapolation of the experimental data to zero temperature. Consequently, in the following analysis $U^{\sigma}(V)$ will be associated with $-E^{\sigma}_{\rm coh}(V)$, with the latter obtained from a fit of the (EX+cRPA)@PBE0 results to the Birch-Murnaghan equation of state [152]

$$E^{\sigma}_{\rm coh}(V) = E^{\sigma}_{0} + \frac{B^{\sigma}_{0} V}{B'^{\sigma}_{0}}\left(\frac{\left(V^{\sigma}_{0}/V\right)^{B'^{\sigma}_{0}}}{B'^{\sigma}_{0}-1}+1\right) - \frac{B^{\sigma}_{0} V^{\sigma}_{0}}{B'^{\sigma}_{0}-1}, \tag{10}$$

where E^{σ}_{0} is the energy at equilibrium, V^{σ}_{0} the equilibrium volume, B^{σ}_{0} the bulk modulus, and B'^{σ}_{0} the derivative of the bulk modulus. As it turned out in the present study, the bulk modulus of Ce_{19} largely overestimates the experimental values of 27 GPa and 19 GPa for the α and γ phases, respectively. This is probably due to the still too small size of the system and affects the estimation of the α-γ phase diagram considerably. Instead, periodic PBE0 calculations produce values of the bulk modulus close to the experimental findings. It was therefore assumed that the bulk modulus B^{σ}_{0} derived from periodic calculations would represent the physical situation better than the cluster B^{σ}_{0}, and it was used in Eq. (9). All other variables are at their (EX+cRPA)@PBE0 values.

In principle, the contribution $S^{\sigma}_{\rm el}$ can be calculated by either integrating over the Kohn-Sham DOS at $T = 0$ K following the Fermi-Dirac distribution, or by introducing electronic temperature effects directly in (EX+cRPA)@PBE0. In the temperature range of interest, i.e. $T < 2000$ K, the latter gives a negligible energy contribution. In our case, at variance with what is observed by Lüders *et al.* [81], also the Fermi-Dirac approach does not change the result considerably. The reason resides in the difference between the PBE DOS, considered by Lüders *et al.*, and the PBE0 α solution. In PBE0, the density of states at the Fermi level is low, Fig. 16. Thus, the integral between the density and the Fermi-Dirac distribution, see Eq. (24) of Ref. [81], varies slowly with temperature.

We add the entropy arising from the magnetic moment of the cerium atoms according to the expression

$$S^{\sigma}_{\rm mag} = k_B \ln(2J+1), \tag{11}$$

where J is the total angular momentum. We here apply Hund's rule, which includes the spin-orbit coupling, $J = m(2l-m)/2$ [153], where l is the orbital angular momentum and m is the magnetic moment. We showed that the magnetic behavior is mainly dictated by the f electrons; therefore we set $l = 3$, and for m use the magnetic moment of the central atom in the two phases of the nineteen-atom cluster.

Estimates for the contribution of lattice vibrations have been provided by some authors, for example by considering the Debye-Grüneisen model [17] or by fitting to experimental data [79]. In this work the vibrational entropy as calculated by Wang *et al.* [83] was included in terms of the difference between the two phases. The authors reported a temperature-independent difference between the phononic contributions of the two phases. So the vibrational entropy was considered to be

$$\Delta S_{\rm vib} = 0.94 k_B. \tag{12}$$

Finally, the concentrations of the two phases are expressed as relative percentages $x^{\gamma} = x_{eq}$ and $x^{\alpha} = (1 - x_{eq})$, and Eq. (5) is evaluated as follows:

$$F(V,T,x_{eq}) = (1-x_{eq})\left[U^{\alpha}(V) - T S^{\alpha}_{\rm mag}\right] + x_{eq}\left[U^{\gamma}(V) - T S^{\gamma}_{\rm mag} - T\Delta S_{\rm vib}\right] - T S_{\rm conf}, \tag{13}$$

where $S_{\rm conf} = -k_B \sum_{\sigma} x^{\sigma} \ln x^{\sigma}$, as obtained in Eq. (8).

The relative percentage of the two phases at equilibrium for a given volume and temperature, calculated from Eq. (7), can be equally obtained [17,79,81] by making the substitution $x_{eq} \to x$ in Eq. (13) with $0 \leqslant x \leqslant 1$, and minimizing the free energy with respect to x. The Helmholtz free energy of cerium as calculated by adding entropic contributions to the (EX+cRPA)@PBE0 results of Ce_{19} is reported in Fig. 17 as a function of volume and relative concentration x of the α and γ phases for six temperatures of interest. For each panel x_{eq} is also reported as a function of volume. At $T = 0$ K the entropic contribution is zero and the free energy is minimized at each volume by the α and γ internal energies in their range of stability. Consequently, x_{eq} is zero for small volumes and approaches one at larger volumes. As the temperature grows, a mixing of the two phases starts to take place in the region between the two equilibrium lattice constants. The relative concentration x_{eq} moves to intermediate values until at high enough temperatures there is no volume for which the system is in a pure α phase.

Following Eq. (13), the free energy of the pseudoalloy is plotted as a function of volume for different values of the temperature in Fig. 18. At $T = 0$ K the free energy coincides with the curves in Fig. 15, except that here the values of the bulk modulus are taken from periodic PBE0 calculations. This produces a slightly different transition pressure of -0.79 GPa, obtained from the double tangent to the curve, still close to the previous value, and in better agreement with the experimental extrapolation to zero temperature $P_t \simeq -0.8$ GPa.

As the temperature grows, the transition pressure moves towards positive values, until at $T = 187$ K it equals zero. The transition temperature at $P_t = 0$ GPa is a quantity of interest, as it represents the lowest point at which direct experimental estimates are available. It was observed that hysteresis effects play an important role in the α-γ phase transition [52]. Moreover, the presence of the β phase further complicates the landscape [6]. Based on the sequence of structural changes that is found in lanthanum, which has no f electrons, the crystal modification from fcc (γ phase) to dhcp (β phase) can be understood in terms of a rearrangement of d electrons. In this case one would think of the f and d electrons as if they would act independently on the properties of the material, the d states not undergoing major changes across the α-γ and α-β transitions, but causing the structural change between the γ and β regions. The f electrons, on the other hand, remain localized in the γ and β phases and are delocalized in the α phase. However, in view of the mutual influence that f and d electrons have on each other, the above considerations cannot be taken for granted; see Ref. [154] for an analysis of the link between d and f electrons and structural changes. Nevertheless, the β-α transition temperature at 0 GPa

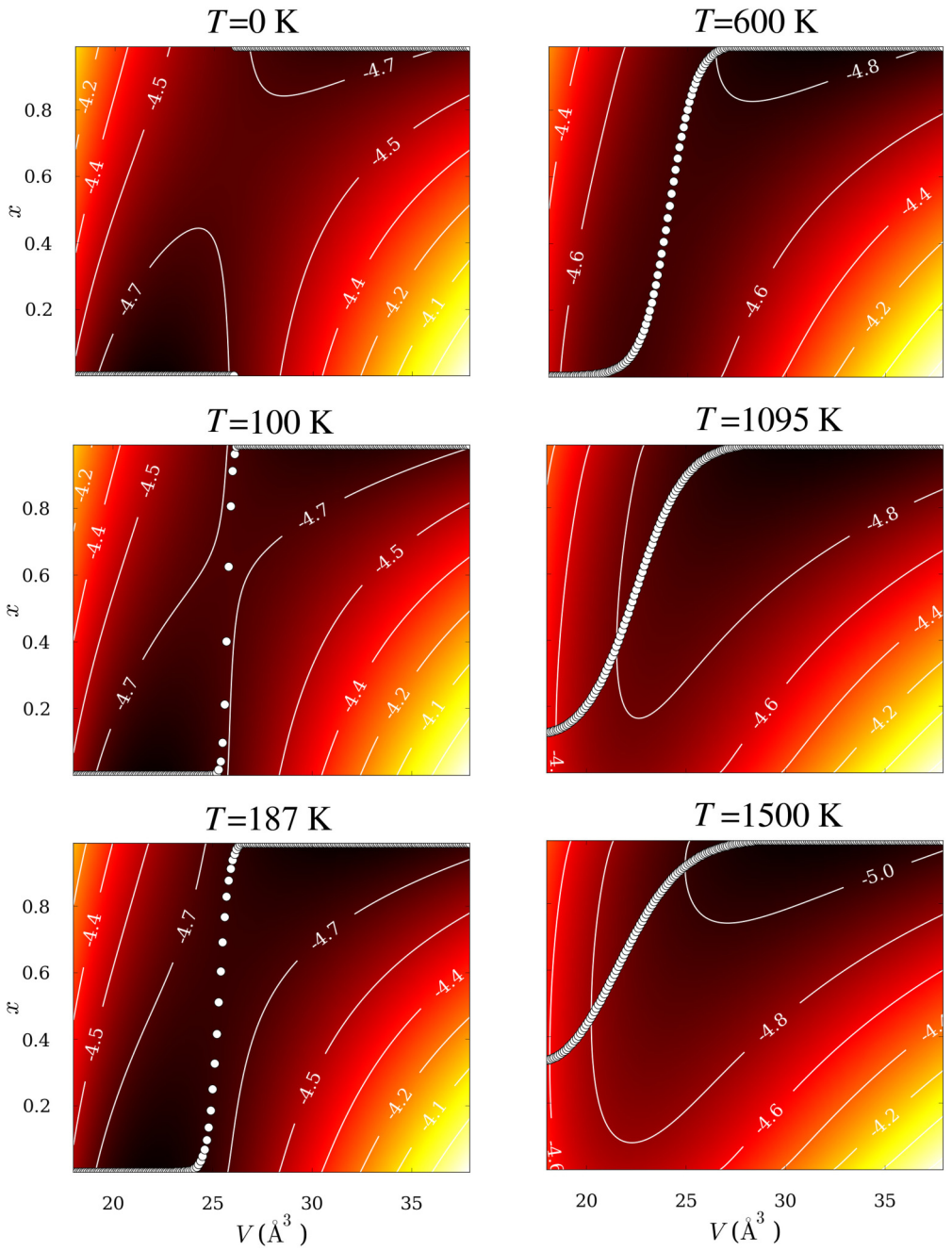

FIG. 17. Calculated Helmholtz free energy as a function of volume and relative concentration of the α and γ phases at six temperatures of interest. For each panel also the equilibrium concentration x_{eq} is plotted as a function of volume. x_{eq} corresponds to the minimum of the free energy.

is accepted as a reasonable estimation for the α-γ phase diagram. As summarized in Table II, $T_0 = 187$ K is not far from the experimental estimation $T_0 = 141$ K [6]. The inclusion of entropic effects in our calculations gives a volume collapse associated with the α-γ phase transition of 28% at room temperature.

In the phase diagram of cerium the α-γ transition line terminates in the β phase at low pressure and in a critical point (C.P.) at $T_c = 460$ K and $P_c = 1.44$ GPa [52]. Also in the present calculations a C.P. manifests. The critical temperature coincides with the disappearance of a negative curvature region in the free energy curve, that, from Fig. 18, appears for $T_c = 1095$. The calculated critical pressure is $P_c = 4.84$ GPa. Previous analysis based on electronic structure theory also reported values close to the ones obtained in this work. Johansson *et al.* found $T_c = 980$ K and $P_c = 3.86$ GPa by means of GGA calculations in which the f electrons were retained in the valence shell in the α phase and in the inert core in the γ phase. Using SIC-LSD Svane *et al.* reported $T_c = 1300$ K and $P_c = 4.7$ GPa and Lüders *et al.* obtained $T_c = 1377$ K and $P_c = 5.6$ GPa. By means of LDA+U calculations, Wang *et al.* found $T_c = 476$ K and $P_c = 2.22$ GPa, but the description of the γ phase was adjusted to the experimental reference through the tunable

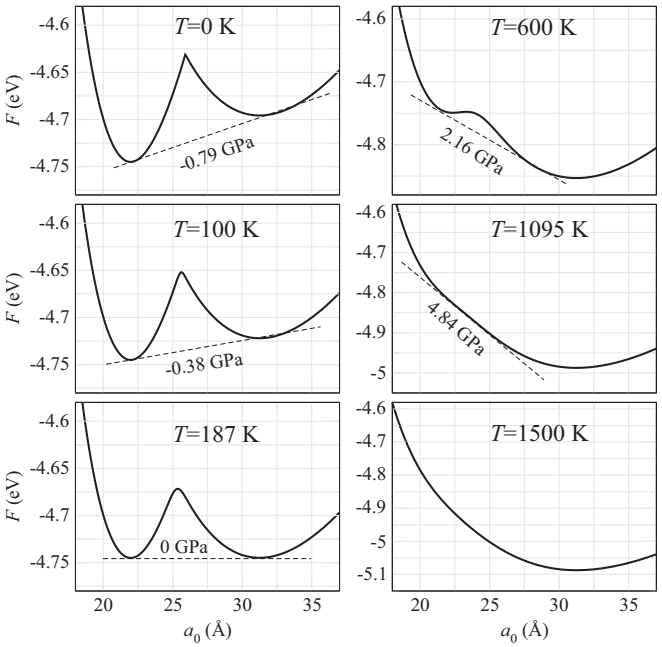

FIG. 18. Calculated Helmholtz free energy as a function of volume for six temperatures of interest and relative equilibrium concentration x_{eq}. In each panel the transition pressure as obtained by the Gibbs construction is also reported. The double tangent to the curves is present until $T_c = 1095$ K. Above that temperature no volume collapse is registered. $T_c = 1095$ K; $P_c = 4.84$ GPa represents the critical point.

U parameter. Our approach differs from the previous ones by the starting point. In our calculations the internal energy at $T = 0$ K is obtained within a single level of theory and no adjustable parameters have been introduced. DMFT studies, which intrinsically include temperature effects, did not report a phase diagram for cerium.

From Eq. (13) it is possible to obtain, at constant T and optimal mixing x_{eq}, the pressure dependence of the volume as

$$P(V,T,x_{eq}) = -\frac{\partial F(V,T,x_{eq})}{\partial V} = -(1-x_{eq})\frac{\partial U^{\alpha}(V)}{\partial V} - (x_{eq})\frac{\partial U^{\gamma}(V)}{\partial V}. \quad (14)$$

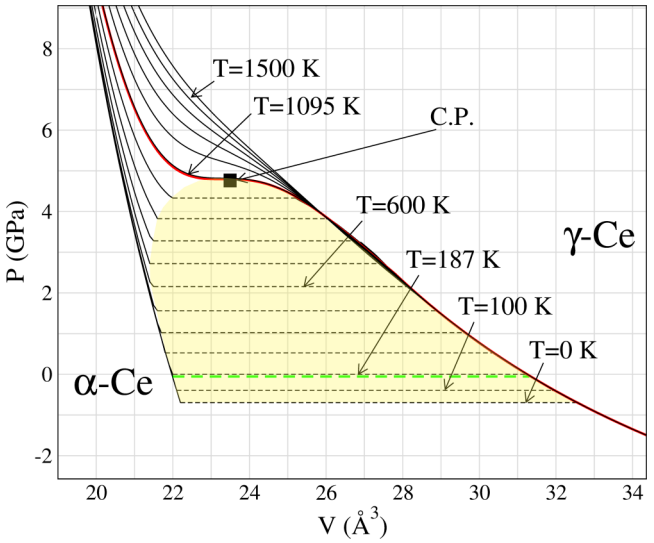

FIG. 19. Calculated pressure versus volume isoterms for temperatures between 0 K, lowest curve, and 1600 K, in steps of 100 K. The results for $T = 187$ K (in green) and $T = 1095$ K (red curve) are also reported as they represent the transition temperature at 0 GPa and the critical point temperature, respectively. C.P. is the critical point.

By inserting Eq. (10) into (14) through the equivalence $U^{\sigma}(V) = -E^{\sigma}_{\rm coh}(V)$, one can further express the pressure explicitly in terms of the coefficients of the Birch-Murnaghan equation of state

$$P(V,T,x_{eq}) = (1-x_{eq})\frac{B_0^{\alpha}}{B_0'^{\alpha}}\left[\left(\frac{V_0}{V}\right)^{B_0'^{\alpha}} - 1\right] + x_{eq}\frac{B_0^{\gamma}}{B_0'^{\gamma}}\left[\left(\frac{V_0}{V}\right)^{B_0'^{\gamma}} - 1\right]. \quad (15)$$

The isoterms that correspond to Eq. (15) are reported in Fig. 19. At each temperature the transition pressure is estimated via the Gibbs construction as reported in Fig. 18. The discontinuities in the P-V curves are indicative of the volume collapse at different temperatures and delimit a region of instability generally known as the *miscibility gap*. The jump in volume between the two phases gradually shrinks with increasing

TABLE II. Results from the present and previous theoretical works and experimental data for the α-γ phase transition. T_0: transition temperature at 0 GPa. P_c: critical pressure. T_c: critical temperature. $\Delta V_{\gamma-\alpha}$: volume collapse associated with the transition at $T = 300$ K.

	Present work	Previous works	Experiments
T_0 (K)	187	135[a], 169[b]	141 ± 10[c]
P_c (GPa)	4.84	3.86[a], 5.6[b], 4.7[d], 2.22[e]	1.96 ± 2[c], 1.8[f], 1.5[g], 1.44[h]
T_c (K)	1095	980[a], 1377[b], 1300[d], 476[e]	600 ± 50[c], 485[f], 480[g], 460[h]
$\Delta V_{\gamma-\alpha}$ (300 K) (%)	28	20[a], 20.5[b], 23.4[d], 16.5[e]	14.7[f], 14[h]

[a]Johansson *et al.*, GGA [17].
[b]Lüders *et al.*, SIC-LSD [81].
[c]Koskenmaki *et al.*, exp. [6].
[d]Svane *et al.*, SIC-LSD [79].
[e]Wang *et al.*, LDA+U [83].
[f]Schiwek *et al.*, exp. [155].
[g]Lipp *et al.*, exp. [15].
[h]Decremps *et al.*, exp. [52].

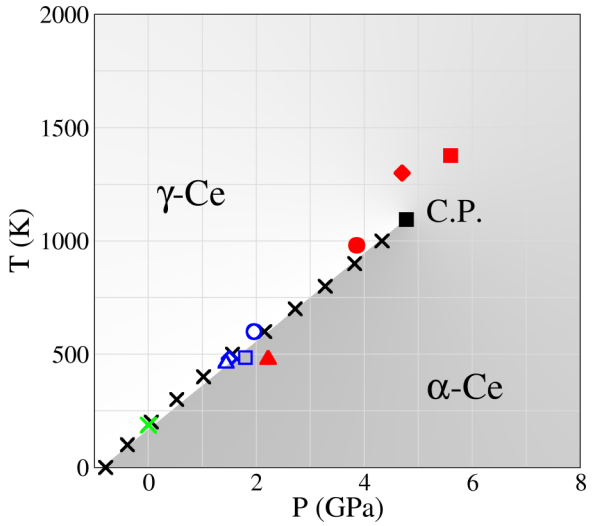

FIG. 20. Calculated temperature-pressure phase diagram of cerium (black crosses) as obtained by adding entropic contributions to the (EX+cRPA)@PBE0 results. C.P. is the calculated critical point (black square). The green cross indicates the transition temperature at $P_t = 0$. Experimental results for C.P., identified by the blue symbols, are from Koskenmaki *et al.* [6,139] (open circle), Schiwek *et al.* [155] (open square), Lipp *et al.* [15] (open diamond, obscured by the triangle), and Decremps *et al.* [52] (open triangle). Previous theoretical data are reported in red from Johansson *et al.* [17] (filled circle), Lüders *et al.* [81] (filled square), Svane *et al.* [79] (filled diamond), and Wang *et al.* [83] (filled triangle).

temperature, until at $T_c = 1095$ K the isoterm becomes smooth and the volume varies continuously with pressure. This determines the critical point of the phase transition, at the associated transition pressure $P_c = 4.84$.

Finally, by plotting the transition temperature as a function of pressure, the phase diagram of the α-γ phase transition can be drawn; see Fig. 20. With respect to the experimental phase diagram, see Fig. 1, the transition line is extended to negative pressures. This is a natural consequence of the fact that in our calculations the phase transition can be described at $T = 0$ K. Due to the lack of experimental references the survival of the phase transition in the negative pressure region has been a matter of debate. A first problematic aspect is the presence of the β phase. In addition, some authors suggested other possible reasons for the disappearance of the phase transition. De Medici *et al.* [156] for example proposed that delocalization of f electrons via a Mott transition mechanism would be suppressed by Kondo screening at low enough temperatures. The present calculations show, however, that a phase diagram can be produced in close resemblance to experiment by adding entropic contributions to the $T = 0$ K internal energy.

The estimated position of the critical point is quite distant from the one reported in experiments. Eventually, introducing the effect of spin-orbit coupling could lead to a renormalization of the temperature, as suggested by Bieder *et al.* [92]. Nevertheless, it is a considerable achievement that the experimental critical points fall on the calculated transition line. This is also expected from the fact that the extrapolated transition pressure to zero temperature agrees well with the calculated one. We find that the transition line displays a linear behavior, which is also observed experimentally. In this sense the present outcome further strengthens the previous conclusion that the difference of the α phase with respect to the γ phase can be understood in terms of "direct" delocalization of f electrons.

VII. SUMMARY AND PERSPECTIVES

Hybrid functional calculations with no constraints produce multiple, distinct solutions for both bulk cerium and cerium clusters at zero temperature. The same behavior can be recovered in PBE by imposing magnetic moment constraints on the system. The hybrid functional solutions can be discriminated by their magnetic moment and the degree of f-electron localization and have been associated with the α and γ phases of cerium. An analysis of the band structure and the electronic density distribution of the two solutions for different magnetic configurations proved that hybrid functionals capture a change in the f wave functions around the region of the experimental α and γ lattice constants. This cannot be reproduced within PBE calculations. A first consequence of this result is that the debate on whether the α-γ phase transition would survive at low temperature or not could be resolved in favor of the former hypothesis. It is one of the main achievements of this work that both phases can be reproduced, at zero temperature, within a single theoretical framework, even if the spectral properties are not well reproduced within hybrid functionals. In fact, DFT is a ground state theory, and the right electronic excitation spectrum is not needed to account for the structural properties of the two phases at zero temperature.

At the hybrid functional level, the energetic ordering of the two solutions is reversed compared to the zero temperature extrapolation. Including correlation effects at the level of the EX+cRPA approach is then essential to rectify this failure and recovers the right ordering, which highlights the role of correlation in rare-earth systems. The nineteen-atom cluster provides a good foundation for reproducing the cerium phase diagram, which is obtained by adding entropy contributions and allowing the two phases to mix at finite temperature. The calculated finite temperature phase diagram is in reasonable agreement with experimental evidence, preserving the linearity of the transition line.

Based on the analysis of the band structure and the electronic density, hybrid functional results appear consistent with a Mott transition scenario, in particular, with the Mott interpretation of localized and delocalized f states in the γ and α phases, respectively. However, we know that the transition is complex, and different mechanisms may cooperate. Our results do not rule out the importance of Kondo physics at finite temperatures. They suggest, rather, that the driving mechanism of the volume collapse should already occur at zero temperature, and therefore could be more directly related to the hybridization between f states.

At the same time, our conclusions do not exclude, see Sec. V A, a quadrupolar charge density alignment in the α phase. Spin unpolarized hybrid functional calculations for

cerium bulk demonstrate that the emergence of the two solutions is linked to a change in the wave functions. In addition, the charge density difference between the solutions shows that there are preferred directions along which the f electron density tends to align. One future goal is therefore to increase the dimension of the unit cell. This would allow the system to explore more degrees of freedom in the quantum mechanical calculations and might provide insight into the possible relevance of the quadrupolar symmetry of the charge density suggested by Nikolaev *et al.* [61].

ACKNOWLEDGMENTS

This work was supported by the Academy of Finland through its Centres of Excellence Programme under Projects No. 251748 and No. 284621. A.R. acknowledges financial support from the European Research Council Advanced Grant DYNamo (ERC-2010-AdG-267374), Ministerio de Economía y Competitividad No. FIS2013-46159-C3-1-P, Grupos Consolidados UPV/EHU del Gobierno Vasco (IT578-13), European Community FP7 project CRONOS (Grant No. 280879-2), and COST Actions No. CM1204 (XLIC) and No. MP1306 (EUSpec).

[1] A. K. Mcmahan, C. Huscroft, R. T. Scalettar, and E. L. Pollock, J. Comput.-Aided Mater. Des. **5**, 131 (1998).
[2] B. I. Min, H. J. F. Jansen, T. Oguchi, and A. J. Freeman, Phys. Rev. B **34**, 369 (1986).
[3] O. Eriksson, M. S. S. Brooks, and B. Johansson, Phys. Rev. B **41**, 7311 (1990).
[4] P. Söderlind, O. Eriksson, B. Johansson, and J. M. Wills, Phys. Rev. B **50**, 7291 (1994).
[5] T. Jarlborg, E. G. Moroni, and G. Grimvall, Phys. Rev. B **55**, 1288 (1997).
[6] D. C. Koskenmaki and K. A. Gschneidner, *Handbook on the Physics and Chemistry of Rare Earths* (North-Holland, Amsterdam, 1978).
[7] M. Casadei, X. Ren, P. Rinke, A. Rubio, and M. Scheffler, Phys. Rev. Lett. **109**, 146402 (2012).
[8] A. D. Becke, J. Chem. Phys. **98**, 5648 (1993).
[9] J. P. Perdew, M. Ernzerhof, and K. Burke, J. Chem. Phys. **105**, 9982 (1996).
[10] J. Heyd, G. E. Scuseria, and M. Ernzerhof, J. Chem. Phys. **118**, 8207 (2003).
[11] D. Langreth and J. Perdew, Solid State Commun. **17**, 1425 (1975).
[12] F. Furche, J. Chem. Phys. **129**, 114105 (2008).
[13] A. Heßelmann and A. Görling, Mol. Phys. **109**, 2473 (2011).
[14] X. Ren, P. Rinke, C. Joas, and M. Scheffler, J. Mater. Sci. **47**, 7447 (2012).
[15] M. J. Lipp, D. Jackson, H. Cynn, C. Aracne, W. J. Evans, and A. K. McMahan, Phys. Rev. Lett. **101**, 165703 (2008).
[16] B. Johansson, Philos. Mag. **30**, 469 (1974).
[17] B. Johansson, I. A. Abrikosov, M. Aldén, A. V. Ruban, and H. L. Skriver, Phys. Rev. Lett. **74**, 2335 (1995).
[18] J. W. Allen and R. M. Martin, Phys. Rev. Lett. **49**, 1106 (1982).
[19] J. W. Allen and L. Z. Liu, Phys. Rev. B **46**, 5047 (1992).
[20] A. Georges, W. Krauth, and M. J. Rozenberg, Rev. Mod. Phys. **68**, 13 (1996).
[21] K. Held, C. Huscroft, R. T. Scalettar, and A. K. McMahan, Phys. Rev. Lett. **85**, 373 (2000).
[22] K. Held and R. Bulla, Eur. Phys. J. B **17**, 7 (2000).
[23] B. Amadon and A. Gerossier, Phys. Rev. B **91**, 161103 (2015).
[24] B. Amadon, F. Jollet, and M. Torrent, Phys. Rev. B **77**, 155104 (2008).
[25] M. MacPherson, G. Everett, D. Wohlleben, and M. Maple, Phys. Rev. Lett. **26**, 20 (1971).
[26] A. Grimberg, C. Schinkel, and A. Zandee, Solid State Commun. **11**, 1579 (1972).
[27] D. Koskimaki and K. Gschneidner, Phys. Rev. B **11**, 4463 (1975).
[28] R. Colvin, S. Arajs, and J. Peck, Phys. Rev. **122**, 14 (1961).
[29] M. K. Wilkinson, H. R. Child, C. J. McHargue, W. C. Koehler, and E. O. Wollan, Phys. Rev. **122**, 1409 (1961).
[30] C. Burr and S. Ehara, Phys. Rev. **149**, 551 (1966).
[31] A. P. Murani, S. J. Levett, and J. W. Taylor, Phys. Rev. Lett. **95**, 256403 (2005).
[32] Stoner suggested in 1934 that an attractive contribution $E_{ex} = -I/4M^2$ (where M is the magnetic polarization and I is a material-dependent parameter) should be considered in order to describe the effect that localized electrons prefer to align their spin when close to each other [157] .
[33] D. Gustafson and A. Mackintosh, J. Phys. Chem. Solids **25**, 389 (1964).
[34] U. Kornstädt, R. Lässer, and B. Lengeler, Phys. Rev. B **21**, 1898 (1980).
[35] A. P. Murani, Z. A. Bowden, A. D. Taylor, R. Osborn, and W. G. Marshall, Phys. Rev. B **48**, 13981 (1993).
[36] J. W. van der Eb, A. B. Kuz'menko, and D. van der Marel, Phys. Rev. Lett. **86**, 3407 (2001).
[37] D. M. Wieliczka, C. G. Olson, and D. W. Lynch, Phys. Rev. B **29**, 3028 (1984).
[38] F. Patthey, B. Delley, W. D. Schneider, and Y. Baer, Phys. Rev. Lett. **55**, 1518 (1985).
[39] E. Weschke, C. Laubschat, T. Simmons, M. Domke, O. Strebel, and G. Kaindl, Phys. Rev. B **44**, 8304 (1991).
[40] J. J. Joyce, A. J. Arko, J. Lawrence, P. C. Canfield, Z. Fisk, R. J. Bartlett, and J. D. Thompson, Phys. Rev. Lett. **68**, 236 (1992).
[41] L. Z. Liu, J. W. Allen, O. Gunnarsson, N. E. Christensen, and O. K. Andersen, Phys. Rev. B **45**, 8934 (1992).
[42] E. Weschke, A. Hohr, G. Kaindl, S. L. Molodtsov, S. Danzenbacher, M. Richter, and C. Laubschat, Phys. Rev. B **58**, 3682 (1998).
[43] M. Higashiguchi, K. Shimada, T. Narimura, H. Namatame, and M. Taniguchi, Phys. B (Amsterdam, Neth.) **351**, 256 (2004).
[44] D. Wieliczka, J. H. Weaver, D. W. Lynch, and C. G. Olson, Phys. Rev. B **26**, 7056 (1982).
[45] Y. Baer and G. Busch, Phys. Rev. Lett. **31**, 35 (1973).
[46] Y. Baer and G. Busch, J. Electron Spectrosc. Relat. Phenom. **5**, 611 (1974).
[47] E. Wuilloud, H. R. Moser, W. D. Schneider, and Y. Baer, Phys. Rev. B **28**, 7354 (1983).
[48] M. Grioni, P. Weibel, D. Malterre, Y. Baer, and L. Du'o, Phys. Rev. B **55**, 2056 (1997).
[49] C. Dallera, M. Grioni, A. Palenzona, M. Taguchi, E. Annese, G. Ghiringhelli, A. Tagliaferri, N. B. Brookes, T. Neisius, and L. Braicovich, Phys. Rev. B **70**, 085112 (2004).

[50] J.-P. Rueff, C. F. Hague, J.-M. Mariot, L. Journel, R. Delaunay, J.-P. Kappler, G. Schmerber, A. Derory, N. Jaouen, and G. Krill, Phys. Rev. Lett. **93**, 067402 (2004).

[51] B. Amadon, S. Biermann, A. Georges, and F. Aryasetiawan, Phys. Rev. Lett. **96**, 066402 (2006).

[52] F. Decremps, L. Belhadi, D. L. Farber, K. T. Moore, F. Occelli, M. Gauthier, A. Polian, D. Antonangeli, C. M. Aracne-Ruddle, and B. Amadon, Phys. Rev. Lett. **106**, 065701 (2011).

[53] I.-K. Jeong, T. W. Darling, M. J. Graf, T. Proffen, R. H. Heffner, Y. Lee, T. Vogt, and J. D. Jorgensen, Phys. Rev. Lett. **92**, 105702 (2004).

[54] M. E. Manley, R. J. McQueeney, B. Fultz, T. Swan-Wood, O. Delaire, E. A. Goremychkin, J. C. Cooley, W. L. Hults, J. C. Lashley, R. Osborn, and J. L. Smith, Phys. Rev. B **67**, 014103 (2003).

[55] F. Decremps, D. Antonangeli, B. Amadon, and G. Schmerber, Phys. Rev. B **80**, 132103 (2009).

[56] D. Antonangeli, D. L. Farber, C. M. Aracne, D. G. Ruddle, J. Siebert, and B. P. Bonner, High Press. Res. **30**, 151 (2010).

[57] M. Krisch, D. L. Farber, R. Xu, D. Antonangeli, C. M. Aracne, A. Beraud, T.-C. Chiang, J. Zarestky, D. Y. Kim, E. I. Isaev, R. Ahuja, and B. Johansson, Proc. Natl. Acad. Sci. USA **108**, 9342 (2011).

[58] F. Porsch and W. B. Holzapfel, Phys. Rev. Lett. **70**, 4087 (1993).

[59] Y. C. Zhao, F. Porsch, and W. B. Holzapfel, Phys. Rev. B **52**, 134 (1995).

[60] A.V. Nikolaev and K. Michel, Eur. Phys. J. B **9**, 619 (1999).

[61] A. Nikolaev, Eur. Phys. J. B **17**, 15 (2000).

[62] A. V. Nikolaev and K. H. Michel, Phys. Rev. B **66**, 054103 (2002).

[63] A. V. Tsvyashchenko, A. V. Nikolaev, A. I. Velichkov, A. V. Salamatin, L. N. Fomicheva, G. K. Ryasny, A. A. Sorokin, O. I. Kochetov, M. Budzynski, and K. H. Michel, Phys. Rev. B **82**, 092102 (2010).

[64] J. Allen, S. Oh, O. Gunnarsson, K. Schönhammer, M. Maple, M. Torikachvili, and I. Lindau, Adv. Phys. **35**, 275 (1986).

[65] M. J. Lipp, A. P. Sorini, J. Bradley, B. Maddox, K. T. Moore, H. Cynn, T. P. Devereaux, Y. Xiao, P. Chow, and W. J. Evans, Phys. Rev. Lett. **109**, 195705 (2012).

[66] A. B. Andrews, J. J. Joyce, A. J. Arko, J. D. Thompson, J. Tang, J. M. Lawrence, and J. C. Hemminger, Phys. Rev. B **51**, 3277 (1995).

[67] A. J. Arko, J. J. Joyce, A. B. Andrews, J. D. Thompson, J. L. Smith, D. Mandrus, M. F. Hundley, A. L. Cornelius, E. Moshopoulou, Z. Fisk, P. C. Canfield, and A. Menovsky, Phys. Rev. B **56**, R7041 (1997).

[68] F. Patthey, W. D. Schneider, M. Grioni, D. Malterre, Y. Baer, and B. Delley, Phys. Rev. Lett. **70**, 1179 (1993).

[69] B. Johansson, A. V. Ruban, and I. A. Abrikosov, Phys. Rev. Lett. **102**, 189601 (2009).

[70] S. V. Streltsov, A. O. Shorikov, and V. I. Anisimov, JETP Lett. **92**, 543 (2010).

[71] P. Morin and D. Schmitt, in *Ferromagnetic Materials*, edited by K. Buschow and E. Wohlfarth (North-Holland, Amsterdam, 1990).

[72] G. Eliashberg and H. Capellmann, JETP Lett. **67**, 125 (1998).

[73] J. P. Perdew and A. Zunger, Phys. Rev. B **23**, 5048 (1981).

[74] S. Kümmel and L. Kronik, Rev. Mod. Phys. **80**, 3 (2008).

[75] A. J. Cohen, P. Mori-Sánchez, and W. Yang, Science (NY) **321**, 792 (2008).

[76] R. Sakuma, T. Miyake, and F. Aryasetiawan, Phys. Rev. B **86**, 245126 (2012).

[77] Z. Szotek, W. M. Temmerman, and H. Winter, Phys. Rev. Lett. **72**, 1244 (1994).

[78] A. Svane, Phys. Rev. Lett. **72**, 1248 (1994).

[79] A. Svane, Phys. Rev. B **53**, 4275 (1996).

[80] J. Laegsgaard and A. Svane, Phys. Rev. B **59**, 3450 (1999).

[81] M. Lüders, A. Ernst, M. Däne, Z. Szotek, A. Svane, D. Ködderitzsch, W. Hergert, B. L. Györffy, and W. M. Temmerman, Phys. Rev. B **71**, 205109 (2005).

[82] A. Shick, J. Electron. Spectrosc. Relat. Phenom. **114-116**, 753 (2001).

[83] Y. Wang, L. G. Hector, H. Zhang, S. L. Shang, L. Q. Chen, and Z. K. Liu, Phys. Rev. B **78**, 104113 (2008).

[84] M. B. Zölfl, I. A. Nekrasov, T. Pruschke, V. I. Anisimov, and J. Keller, Phys. Rev. Lett. **87**, 276403 (2001).

[85] K. Held, A. K. McMahan, and R. T. Scalettar, Phys. Rev. Lett. **87**, 276404 (2001).

[86] A. K. McMahan, K. Held, and R. T. Scalettar, Phys. Rev. B **67**, 075108 (2003).

[87] A. K. McMahan, Phys. Rev. B **72**, 115125 (2005).

[88] K. Haule, V. Oudovenko, S. Y. Savrasov, and G. Kotliar, Phys. Rev. Lett. **94**, 036401 (2005).

[89] A. K. McMahan, R. T. Scalettar, and M. Jarrell, Phys. Rev. B **80**, 235105 (2009).

[90] S. V. Streltsov, E. Gull, A. O. Shorikov, M. Troyer, V. I. Anisimov, and P. Werner, Phys. Rev. B **85**, 195109 (2012).

[91] M. Lavagna, C. Lacroix, and M. Cyrot, Phys. Lett. A **90**, 210 (1982).

[92] J. Bieder and B. Amadon, Phys. Rev. B **89**, 195132 (2014).

[93] N. Lanatà, Y.-X. Yao, C.-Z. Wang, K.-M. Ho, J. Schmalian, K. Haule, and G. Kotliar, Phys. Rev. Lett. **111**, 196801 (2013).

[94] M.-F. Tian, H.-F. Song, H.-F. Liu, C. Wang, Z. Fang, and X. Dai, Phys. Rev. B **91**, 125148 (2015).

[95] J. D. Thompson, Z. Fisk, J. M. Lawrence, J. L. Smith, and R. M. Martin, Phys. Rev. Lett. **50**, 1081 (1983).

[96] N. Devaux, M. Casula, F. Decremps, and S. Sorella, Phys. Rev. B **91**, 081101(R) (2015).

[97] A. D. Becke, J. Chem. Phys. **104**, 1040 (1996).

[98] A. D. Becke, J. Chem. Phys. **98**, 1372 (1993).

[99] M. Levy, Phys. Rev. A **26**, 1200 (1982).

[100] P.-O. Löwdin, Adv. Chem. Phys. **2**, 207 (2007).

[101] J. P. Perdew, K. Burke, and M. Ernzerhof, Phys. Rev. Lett. **77**, 3865 (1996).

[102] J. Paier, R. Hirschl, M. Marsman, and G. Kresse, J. Chem. Phys. **122**, 234102 (2005).

[103] J. Heyd and G. E. Scuseria, J. Chem. Phys. **121**, 1187 (2004).

[104] J. Heyd and G. E. Scuseria, J. Chem. Phys. **120**, 7274 (2004).

[105] K. N. Kudin, G. E. Scuseria, and R. L. Martin, Phys. Rev. Lett. **89**, 266402 (2002).

[106] J. E. Peralta, E. R. Batista, G. E. Scuseria, and R. L. Martin, J. Chem. Theory Comput. **1**, 612 (2005).

[107] P. J. Hay, R. L. Martin, J. Uddin, and G. E. Scuseria, J. Chem. Phys. **125**, 034712 (2006).

[108] M. Casadei, Density-functional theory for f-electron systems: The α-γ phase transition in cerium, Ph.D. thesis, Freie Universitaet Berlin, 2013.

[109] N. Mermin, Phys. Rev. **137**, A1441 (1965).

[110] C. L. Fu and K. M. Ho, Phys. Rev. B **28**, 5480 (1983).

[111] M. Methfessel and A. T. Paxton, Phys. Rev. B **40**, 3616 (1989).

[112] M. Gillan, J. Phys.: Condens. Matter **1**, 689 (1989).
[113] F. Wagner, T. Laloyaux, and M. Scheffler, Phys. Rev. B **57**, 2102 (1998).
[114] H. Fukutome, Prog. Theor. Phys. **45**, 1382 (1971).
[115] B. Meredig, A. Thompson, H. A. Hansen, C. Wolverton, and A. van de Walle, Phys. Rev. B **82**, 195128 (2010).
[116] F. Jollet, G. Jomard, B. Amadon, J. P. Crocombette, and D. Torumba, Phys. Rev. B **80**, 235109 (2009).
[117] D. Bohm and D. Pines, Phys. Rev. **82**, 625 (1951).
[118] D. Pines and D. Bohm, Phys. Rev. **85**, 338 (1952).
[119] D. Pines, Phys. Rev. **92**, 626 (1953).
[120] D. Bohm and D. Pines, Phys. Rev. **92**, 609 (1953).
[121] M. Gell-Mann and K. Brueckner, Phys. Rev. **106**, 364 (1957).
[122] See Ren *et al.* [14] for a recent review on the RPA.
[123] J. Toulouse, I. C. Gerber, G. Jansen, A. Savin, and J. G. Ángyán, Phys. Rev. Lett. **102**, 096404 (2009).
[124] F. Furche and T. Van Voorhis, J. Chem. Phys. **122**, 164106 (2005).
[125] X. Ren, A. Tkatchenko, P. Rinke, and M. Scheffler, Phys. Rev. Lett. **106**, 153003 (2011).
[126] H. Eshuis and F. Furche, J. Phys. Chem. Lett. **2**, 983 (2011).
[127] J. Harl, L. Schimka, and G. Kresse, Phys. Rev. B **81**, 115126 (2010).
[128] J. Harl and G. Kresse, Phys. Rev. Lett. **103**, 056401 (2009).
[129] J. Harl and G. Kresse, Phys. Rev. B **77**, 045136 (2008).
[130] H.-J. Kim, A. Tkatchenko, J.-H. Cho, and M. Scheffler, Phys. Rev. B **85**, 041403 (2012).
[131] J. Ma, Phys. Rev. B **84**, 033402 (2011).
[132] X. Ren, P. Rinke, and M. Scheffler, Phys. Rev. B **80**, 045402 (2009).
[133] M. Rohlfing and T. Bredow, Phys. Rev. Lett. **101**, 266106 (2008).
[134] V. Blum, R. Gehrke, F. Hanke, P. Havu, V. Havu, X. Ren, K. Reuter, and M. Scheffler, Comput. Phys. Commun. **180**, 2175 (2009).
[135] E. van Lenthe, E. J. Baerends, and J. G. Snijders, J. Chem. Phys. **101**, 9783 (1994).
[136] S. V. Levchenko, X. Ren, J. Wieferink, R. Johanni, P. Rinke, V. Blum, and M. Scheffler, Comp. Phys. Comm. **192**, 60 (2015).
[137] FHI-aims NAO basis sets for cerium: tier 1: [Xe]+$2s2p2d2f1g$; tier 2: [Xe]+$3s3p4d3f2g1h$; and tier 3: [Xe]+$4s4p5d5f3g2h$.
[138] T. Jarlborg, Phys. Rev. B **89**, 184426 (2014).
[139] J. Olsen, L. Gerward, U. Benedict, and J. Itié, Physica B+C **133**, 129 (1985).
[140] C. Kittel, *Introduction to Solid State Physics*, 7th ed. (Wiley, New York, 1996).
[141] R. Podloucky and D. Glötzel, Phys. Rev. B **27**, 3390 (1983).
[142] W. E. Pickett, A. J. Freeman, and D. D. Koelling, Phys. Rev. B **23**, 1266 (1981).
[143] M. Scheffler and C. Stampfl, in *Handbook of Surface Science*, edited by K. Horn and M. Scheffler (Elsevier, Amsterdam, 2000), Vol. 2, p. 286.
[144] Q.-M. Hu, K. Reuter, and M. Scheffler, Phys. Rev. Lett. **98**, 176103 (2007).
[145] For the PBE and PBE0 functionals, for which the basis set superposition error (BSSE) [158] can be neglected, E_c^{atom} is always the energy of the free atom. For (EX+cRPA)@PBE/PBE0 the atomic reference must be calculated explicitly at each atom position.
[146] Note that the sum runs from 1 to 12, as 12 is the maximum number of nearest neighbors for an atom in the fcc environment.
[147] A similar change of the magnetic moment with the lattice constant is found for cerium bulk. See Fig. 2 for the explicit volume dependence of the spin.
[148] The spin on each atom is calculated according to the Mulliken charge partitioning scheme [159].
[149] Note that the density difference plot reported in Fig. 7, which, for cerium bulk, provides an indication of the delocalization of f electrons in the α-like phase with respect to the γ phase, displays the same characteristic when obtained from the densities of the two Ce_{19} solutions.
[150] F. Tran, F. Karsai, and P. Blaha, Phys. Rev. B **89**, 155106 (2014).
[151] A coexistence of the two phases is generally observed in experiments; see, e.g., Decremps *et al.* [52] .
[152] F. D. Murnaghan, Proc. Natl. Acad. Sci. USA **30**, 244 (1944).
[153] Y. Wang, Phys. Rev. B **61**, R11863 (2000).
[154] B. Johansson, W. Luo, S. Li, and R. Ahuja, Sci. Rep. **4**, 6398 (2014).
[155] A. Schiwek, High Pressure Res. **22**, 407 (2002).
[156] L. de' Medici, A. Georges, G. Kotliar, and S. Biermann, Phys. Rev. Lett. **95**, 066402 (2005).
[157] G. Stollhoff, A. M. Oleś, and V. Heine, Phys. Rev. B **41**, 7028 (1990).
[158] F. B. van Duijneveldt, J. G. C. M. van Duijneveldt–van de Rijdt, and J. H. van Lenthe, Chem. Rev. **94**, 1873 (1994).
[159] R. S. Mulliken, J. Chem. Phys. **23**, 1833 (1955).